Article

Cell Reports

CDYL Deficiency Disrupts Neuronal Migration and Increases Susceptibility to Epilepsy

Graphical Abstract

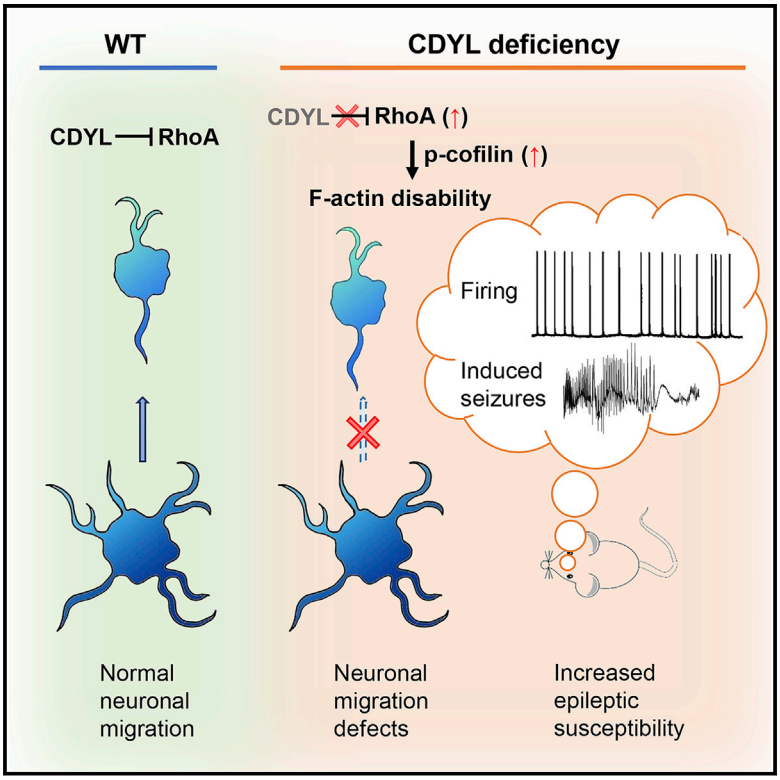

Authors

Rui Qin, Shuai Cao, Tianjie Lyu, Cai Qi, Weiguang Zhang, Yun Wang

Correspondence

wangy66@bjmu.edu.cn

In Brief

Qin et al. find that CDYL plays a role in neuronal migration by repressing RhoA transcription. CDYL deficiency leads to increased excitability of cortical pyramidal neurons and susceptibility to epilepsy in mice.

Highlights

- The transcriptional corepressor CDYL drives neuronal migration in the brain
- CDYL regulates the actin cytoskeleton by transcriptionally repressing RhoA
- CDYL knockdown increases the excitability of cortical pyramidal neurons
- CDYL deficiency specifically increases the susceptibility to epilepsy

Qin et al., 2017, Cell Reports *18*, 380–390
January 10, 2017
http://dx.doi.org/10.1016/j.celrep.2016.12.043

OPEN ACCESS
CellPress

Cell Reports
Article

CDYL Deficiency Disrupts Neuronal Migration and Increases Susceptibility to Epilepsy

Rui Qin,[1,4] Shuai Cao,[1,4] Tianjie Lyu,[1] Cai Qi,[1] Weiguang Zhang,[2] and Yun Wang[1,3,5,*]
[1]Neuroscience Research Institute and Department of Neurobiology, School of Basic Medical Sciences, Key Laboratory for Neuroscience, Ministry of Education/National Health and Family Planning Commission, Peking University, Beijing 100191, China
[2]Department of Anatomy, Histology and Embryology, School of Basic Medical Sciences, Peking University Health Science Center, Beijing 100191, China
[3]PKU-IDG/McGovern Institute for Brain Research, Peking University, Beijing 100871, China
[4]Co-first author
[5]Lead Contact
*Correspondence: wangy66@bjmu.edu.cn
http://dx.doi.org/10.1016/j.celrep.2016.12.043

SUMMARY

During brain development, the correct migration of newborn neurons is one of the determinants of circuit formation, and neuronal migration defects may lead to neurological and psychiatric disorders. The molecular mechanisms underlying neuronal migration and related disorders are poorly understood. Here, we report that Chromodomain Y-like (CDYL) is critical for neuronal migration in mice. Knocking down CDYL caused neuronal migration defects and disrupted both mobility and multipolar-to-bipolar transition of migrating neurons. We find that CDYL regulates neuronal migration by transcriptionally repressing RhoA. In addition, CDYL deficiency increased the excitability of cortical pyramidal neurons and the susceptibility of mice to convulsant-induced seizures. These results demonstrate that CDYL is a regulator of neuronal migration and shed light on the pathogenesis of seizure-related neurodevelopmental disorders.

INTRODUCTION

During the development of the mammalian cerebral cortex, newborn neurons generated from progenitor cells in the ventricular and subventricular zone migrate along the radial glia to the cortical plate (Ayala et al., 2007; Marín and Rubenstein, 2003; Nadarajah et al., 2001). Defects in neuronal migration can lead to neuropsychiatric disorders including schizophrenia, autism, and epilepsy (Deutsch et al., 2010; Gleeson and Walsh, 2000; Guerrini and Parrini, 2010). Although many extrinsic cues, receptors, and intracellular pathways have been found to regulate neuronal migration (Boitard et al., 2015; Morgan-Smith et al., 2014), little is known about how epigenetic mechanisms might contribute to this process.

Chromodomain Y-like (CDYL) is a recently identified transcriptional corepressor that contains an amino-terminal chromodomain and a carboxy-terminal enoyl-coenzyme A hydratase-isomerase catalytic domain, and is a member of the CDY family (Caron et al., 2003; Lahn and Page, 1999). It was first identified as a key player in the regulation of mammalian spermatogenesis (Lahn et al., 2002). Our previous microarray studies indicated that a significant number of CDYL target genes were associated with the development and function of the nervous system, and we found that CDYL negatively regulates dendritic branching in hippocampal neurons (Qi et al., 2014). CDYL is highly expressed in the brain as early as embryonic day 12 and is rapidly degraded during neural development (Figure 1A), suggesting that CDYL may function as a regulator during early stages of neural development, such as neuronal migration.

Generally, radial migration is composed of three steps: polarization of the leading process, nucleokinesis, and the retraction of the trailing process (Marín et al., 2006). In parallel to these events, proper regulation of the cytoskeleton is critical for the movement of projection neurons (Jaglin and Chelly, 2009; Tian et al., 2015; Tsai and Gleeson, 2005). RhoA, a member of the Rho family of GTPases, plays a significant role in cytoskeleton dynamics. It has been identified as downstream of several regulators of neuronal migration, including Rnd2, Rnd3, Mst3, and Gmip (Azzarelli et al., 2014; Ota et al., 2014; Pacary et al., 2011; Tang et al., 2014). Although RhoA activity in neuronal migration has been fully demonstrated, little is known about the regulation of RhoA protein levels during neuronal migration. Studies have shown that genetic deletion of RhoA in the developing cerebral cortex results in two migrational disorders: subcortical band heterotopia and cobblestone lissencephaly (Cappello et al., 2012), whereas overexpression of RhoA causes defects in neuronal migration (Ge et al., 2006; Tang et al., 2014). These findings reveal that the regulation of RhoA protein levels is important for neuronal migration, but the transcriptional machinery responsible for RhoA gene expression during the migration process is unclear.

Here, we report that CDYL is a regulator of neuronal migration and is essential for the formation of functional circuits. Silencing CDYL in utero specifically perturbed the neuronal transition from the multipolar to the bipolar stage and disrupted neuronal migration. CDYL repressed RhoA transcription, stabilizing the cytoskeletal activity required to orchestrate the six-layered laminar structure of the cortex. CDYL-silenced neurons showed aberrant

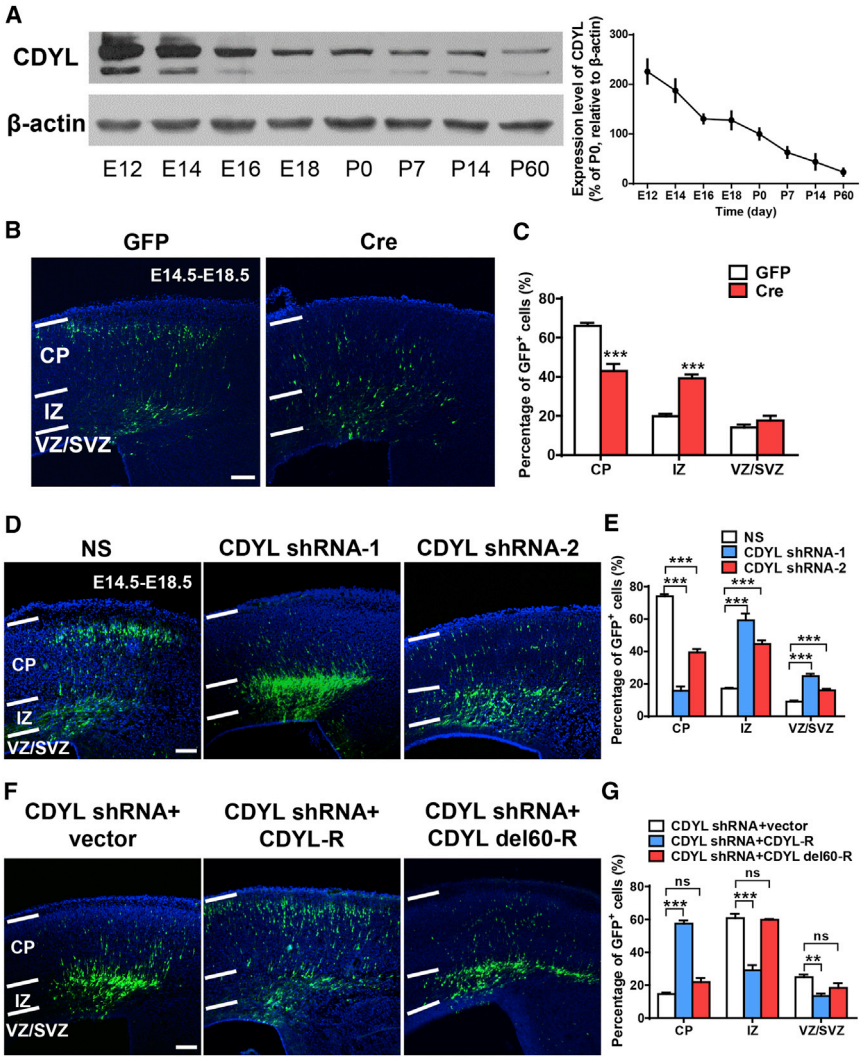

Figure 1. CDYL Is Important for Neuronal Migration during Brain Development

(A) Expression of CDYL in brain at different developmental stages (E12 to P60, left) and quantification (right). ***p < 0.001, one-way ANOVA. The experiment was repeated at least three times.

(B) Representative brain slices of *Cdyl*$^{F/F}$ mice with Cre or GFP plasmids. Mice were in utero electroporated at E14.5 and were sacrificed at E18.5. Scale bar, 100 μm.

(C) Quantification of the distribution of the GFP-positive neurons. ***p < 0.001, two-way ANOVA with Bonferroni post hoc test.

(D) Representative slices of brains in utero electroporated at E14.5 with non-silencing (NS) or CDYL shRNA for 4 days. The cells were co-transfected with GFP to visualize the distribution of transfected neurons (green), and cell nuclei were stained with Hoechst (blue). Scale bar, 100 μm.

(E) Quantification of the distribution of the GFP-positive neurons. ***p < 0.001, two-way ANOVA with Bonferroni post hoc test.

(F) Representative brain slices with in utero electroporation of CDYL shRNA together with vector, CDYL-resistant (CDYL-R) or CDYL del60-R. Scale bar, 100 μm.

(G) Quantification of the distribution of GFP-positive neurons. **p < 0.01; ***p < 0.001; ns, no statistical significance; two-way ANOVA with Tukey post hoc test. More than 1,000 neurons from three to five brains were analyzed in each group. Data are presented as mean ± SEM.

intrinsic excitability and synaptic connectivity, and the deficient mice showed increased seizure susceptibility when treated with a convulsant. Our findings thus reveal a transcriptional pathway that is critical for cortical development.

RESULTS

CDYL Is Essential for Neuronal Migration Dependent on Its Association with Chromatin Histones

To understand the role of CDYL in cortical development, we first examined its expression in the mouse cortex at different developmental stages (Figure 1A). The protein abundance of CDYL decreased during the maturation of the cortex, with the highest level present at embryonic days (E) 14–18, during which most cortical projection neurons in the cortical plate (CP) region migrate. Subsequently, we explored whether CDYL was involved in neuronal migration. First, we performed gain-of-function experiments, overexpression of CDYL constructs together with GFP by in utero electroporation (IUE) into E14.5 mouse brains for 4 days. The results showed that overexpression of CDYL did not affect neuronal migration (Figures S1A and S1B). Then the loss-of-function strategy was used, immunostaining for Cux1, a marker for layers II–IV, to examine the migration behavior in the cerebral cortex of *Cdyl* conditional knockout (cKO) mice (Figures S1C–S1E) by crossing homozygous *Cdyl*-loxP mice with *Emx1-Cre* (cerebral-cortex-specific knockout) (Guo et al., 2000). In *Cdyl* cKO mice, many Cux1-positive cells remained in the intermediate zone (IZ) at postnatal day (P) 2 (Figures S1F and S1G). In addition, the migration defects were found in the electroporation of GFP into the *Cdyl* cKO mouse (Figures S1H and S1I), and acute deletion of CDYL by IUE of the Cre construct together with GFP into brains of *Cdyl*$^{F/F}$ mice at E14.5 resulted in a defect in the radial migration at E18.5 when compared with electroporation of only GFP (Figures 1B and 1C), with all the results together demonstrating that CDYL is required for proper neuronal migration in the embryonic cortex. Finally, we used a short hairpin RNA (shRNA) approach: two shRNAs (CDYL shRNA-1 or shRNA-2) specifically targeting CDYL (Figures S1J and S1K) or non-silencing (NS) shRNA was co-electroporated with a GFP construct into mice progenitor cells at E14.5 by IUE. After 4 days, we analyzed the distribution of GFP-positive cells in the cortical wall. Most of the neurons expressing control shRNA migrated into the upper regions of the

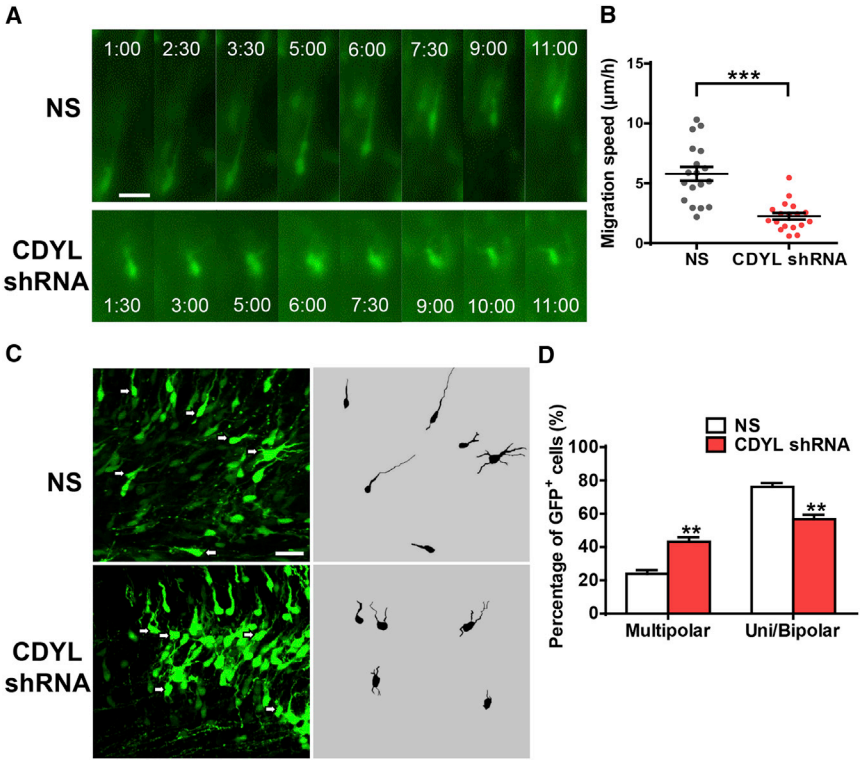

Figure 2. CDYL Controls the Motility and Multipolar-to-Bipolar Transition of Migrating Neurons

(A) Mouse brains were electroporated in utero with control (NS) or CDYL shRNA plasmids, and GFP plasmids were cotransfected to visualize the morphology of the neurons analyzed. After 3 days, brains were sectioned and cultured. Live-cell imaging was performed on the cells in the IZ for at least 11 hr. Scale bar, 20 μm.

(B) Quantification of migration speeds of neurons transfected with control or CDYL shRNA during the 11 hr monitoring, n = 18, 18 neurons from three mice for each group. Selection and analysis of representative cells among all the neurons in videos were randomized and observer blinded. Mann-Whitney test, ***$p < 0.001$.

(C) Knocking down CDYL disrupted the neuronal morphology in vivo. Right: drawings of representative neurons denoted by arrows in the left panels. Scale bar, 20 μm.

(D) Quantification of the percentages of neurons with unipolar or bipolar morphology and multipolar processes. **$p < 0.01$, two-way ANOVA with Bonferroni post hoc test. More than 100 GFP-positive neurons from at least three brains were analyzed in each group. Data are presented as mean ± SEM.

CP, whereas knockdown of CDYL by either CDYL shRNA-1 or CDYL shRNA-2 led to accumulation of migrating neurons in the intermediate zone (IZ) and the ventricular zone/subventricular zone (VZ/SVZ) (Figures 1D and 1E). In further CDYL knockdown experiments, CDYL shRNA-1 was used and was described as CDYL shRNA.

To exclude the possible off-target effects of the shRNA system, we performed rescue experiments. Co-expression of CDYL-R that was resistant to CDYL shRNA (Figure S1L) restored the migration defects at E18.5. However, the N-terminal sequence of 60 amino acid (the chromodomain) deletion mutant CDYL (CDYL del60-R) could not correct the migration defects (Figures 1F and 1G), suggesting that CDYL regulates neuronal migration dependent on its association with chromatin histones.

CDYL Regulates the Motility and the Multipolar-to-Bipolar Transition of Migratory Neurons

During the migration of cortical pyramidal neurons to their terminal positions, one of the most important processes is the change in morphology of radially migrating neurons from multipolar to bipolar while in the intermediate zone (Ip et al., 2011; Kriegstein and Noctor, 2004; Tabata et al., 2009). To study the migratory behavior of neurons with CDYL knockdown, we performed time-lapse experiments using slices of brain tissue. NS or CDYL shRNA was electroporated into the developing cortex together with GFP to label the electroporated cells at E14.5 for 3 days. Then organotypic cortical slices were prepared for live-imaging analysis. More neurons expressing NS shRNA exhibited bipolar morphology and migrated through the intermediate zone to the cortical plate (Movie S1), whereas more neurons with CDYL shRNA retained a multipolar morphology and stayed in the intermediate zone (Movie S2). We further noted that the neurons expressing CDYL shRNA in the IZ migrated more slowly than neurons expressing NS shRNA (Figures 2A and 2B).

In addition to migration defects, knocking down CDYL also resulted in abnormal neuronal morphologies. We performed IUE at E14.5 and analyzed the neuronal morphology at different layers 3 days later. In the IZ and CP, fewer CDYL-knockdown neurons (averaged 56.73% compared with 76.13% of NS) displayed a bipolar or unipolar morphology with one leading process toward the pia surface and a trailing process oriented below. By contrast, a larger percentage (43.24% compared with 23.87% in NS) of CDYL-silenced neurons in the IZ showed round or multipolar shapes with multiple and complex neurites (Figures 2C and 2D).

Having established the critical role of CDYL in neuronal migration and neural morphology in vivo, we next investigated the functions of CDYL in vitro. To study the functions of CDYL at the cellular level, we electroporated CDYL shRNA together with GFP into the cerebral cortex at E14.5; after 48 hr, the electroporated cortex was digested and cultured. Neuronal morphology was analyzed 3 days later. Compared with the control neurons, which developed into polarized neurons with a unique leading neurite each, development of polarization was hindered in CDYL-knockdown neurons. Furthermore, the developmental defects were reversed by the addition of CDYL-R (Figures S2A and S2B). We also investigated the growth of callosal axons at P7. In the control group, bundles of GFP-positive axons

passed through the midline and projected to the contralateral cortex. In P7 mice from the CDYL shRNA group, the axon terminals had not extended as far as in the control mice (Figure S2C). Altogether, these results suggest that CDYL is required for axon extension and refinement both in vitro and in vivo.

CDYL Knockdown Does Not Alter the Fate of the Cortical Neurons

To test whether the migration defects of the CDYL-knockdown neurons were due to cell death or to changes in cell fate, we examined the identity of CDYL-silenced ectopic neurons. The nestin-labeled radial glia scaffold, along which the cortical projection neurons migrated, was not affected by knocking down CDYL (Figure S3A). Loss of CDYL did not induce the apoptosis or the proliferation of the cortical progenitor cells, which were labeled by the apoptosis marker activated caspase-3 (Figure S3B) and the cell cycle marker Ki67 (Figure S3C), respectively.

At P7, control neurons have arrived at the cortical plate; in contrast, the majority of CDYL-silenced neurons remained in layers V and VI and in the white matter (WM). These ectopic neurons were positive for the layer II-IV marker Cux1 and negative for the layer V-VI marker Tbr1 (Figures S4A and S4B). These results indicated that CDYL knockdown interfered specifically and cell autonomously with neuronal migration.

CDYL Regulates Neuronal Migration and Neuronal Polarization by Stabilizing the Actin Cytoskeleton

Next, we studied the mechanism by which CDYL regulates neuronal migration and neurite growth. Several studies have reported that the precise regulation of cytoskeletal components is critical for nuclear translocation and cell morphology during neuronal migration (Jaglin and Chelly, 2009; Marín et al., 2010; Tsai and Gleeson, 2005). Because our results showed that CDYL regulates neuronal migration in a specific and cell-autonomous manner, we hypothesized that the stability of the actin cytoskeleton may be defective in CDYL-silenced neurons. To clarify this possibility, we electroporated NS or CDYL shRNA into the embryonic cortex. At 48 hr after electroporation, the cortex was digested and plated in the cell dishes, and the actin cytoskeleton was stained with rhodamine-labeled phalloidin after 24 hr in culture. In the control neurons, there was an obvious growth cone with an enrichment of F-actin at the leading edge (Figure 3A), but in the neurons with CDYL knockdown, the growth cone was branched (Figure 3B), and the F-actin was not centralized as in the control group. Furthermore, we observed that the phosphorylation of cofilin, an F-actin severing factor, increased after knockdown CDYL (Figure 3C). As we had expected, F-actin was again central in the growth cone when cells expressed cofilin S3A, a nonphosphorylatable form of cofilin that constitutively depolymerizes F-actin (Figure 3D; Figure S5A).

RhoA Acts Downstream of CDYL during Neuronal Migration

Because the small GTPase protein RhoA is well-known to function as a regulator of the actin cytoskeleton (Govek et al., 2005; Ridley et al., 2003), we investigated whether RhoA is involved in CDYL-mediated actin polymerization. The luciferase reporter-gene assay showed that knockdown of CDYL increased the transcriptional activity of RhoA (Figure 4A). Next, we examined the mRNA and protein levels of RhoA in CDYL-silenced cortical neurons. Quantitative real-time PCR and western blot analysis showed that both the mRNA and the protein levels of RhoA were upregulated by the knockdown of CDYL (Figures 3C and 4B). Similar results were also detected in N2a cells (Figures S5B and S5C). RhoA shrNA effectively knocked down RhoA expression and was able to abolish the upregulation of RhoA expression induced by knocking down CDYL (Figures S5D–S5F).

To determine whether repressing RhoA transcription is responsible for the neuronal migration defects of the CDYL-silenced neurons, we co-electroporated CDYL shRNA and GFP with either RhoA shRNA or cofilin S3A into E14.5 mouse brains (Figures 4C and 4D). Both RhoA shRNA and cofilin S3A could rescue the migration defects induced by silencing CDYL (Figures 4E and 4F), thus indicating that CDYL promotes neuronal migration by repressing RhoA transcription, and thereby stabilizing the actin cytoskeleton.

Loss of CDYL Increases Susceptibility to Pentylenetetrazol-Induced Seizures in Mice

Abnormal neurodevelopment contributes to a variety of neurological and psychiatric disorders, such as intellectual disability and epilepsy (Braat and Kooy, 2015). To further investigate the requirement for CDYL in normal neural functions, we screened the possible behavioral deficits resulting from CDYL deficiency. The convulsant agent pentylenetetrazol (PTZ) was used to induce seizures in the wild-type (WT), *Emx1-Cre* (Cre), *Cdyl*$^{F/+}$:*Emx1-Cre* heterozygotes (Heter), and *Cdyl*$^{F/F}$:*Emx1-Cre* conditional knockout (cKO) mice, and the epilepsy-like firing patterns were recorded with electroencephalography (EEG) to confirm the high sensitivity and accuracy of the behavioral observations used for seizure detection (Figure 5A). The cumulative doses of PTZ and the latency to induce the onset of generalized tonic-clonic seizures were significantly lower in Heter and cKO mice (Figures 5B and 5C). Notably, the intervals between the minimal and tonic-clonic seizures in the Heter and cKO mice were significantly longer than those in WT and Cre mice (Figure 5D). Consistent with this, in utero knockdown of CDYL also aggravated seizure susceptibility (Figures 5E–5G). These results suggest that CDYL deficiency increases the susceptibility of mice to PTZ-induced seizures.

In addition, other behavioral tests were used to examine the function of CDYL in motor ability, normal emotional state, learning, and memory. Heter and cKO mice exhibited no obvious motor disability in a 5-day motor learning paradigm (Figure S6A), and they behaved normally in the open field test (OFT) (Figures S6B and S6C) and elevated plus maze (EPM) (Figures S6D–S6F). In context-dependent and cue-dependent fear conditioning tests, the total freezing times of Heter and cKO mice showed no differences from those of WT and Cre mice in both the training and the test stages (Figures S6G–S6J). We also used the Morris water maze (MWM) to test the spatial learning and memory of mice (Figure S7A). In the 5-day training phase in MWM, Heter and cKO mice exhibited normal learning ability (Figure S7B). On the test day, no significant deficiency of spatial acquisition of memory was observed in Heter and cKO mice (Figures S7C–S7E). Consistent with the above examinations of locomotor

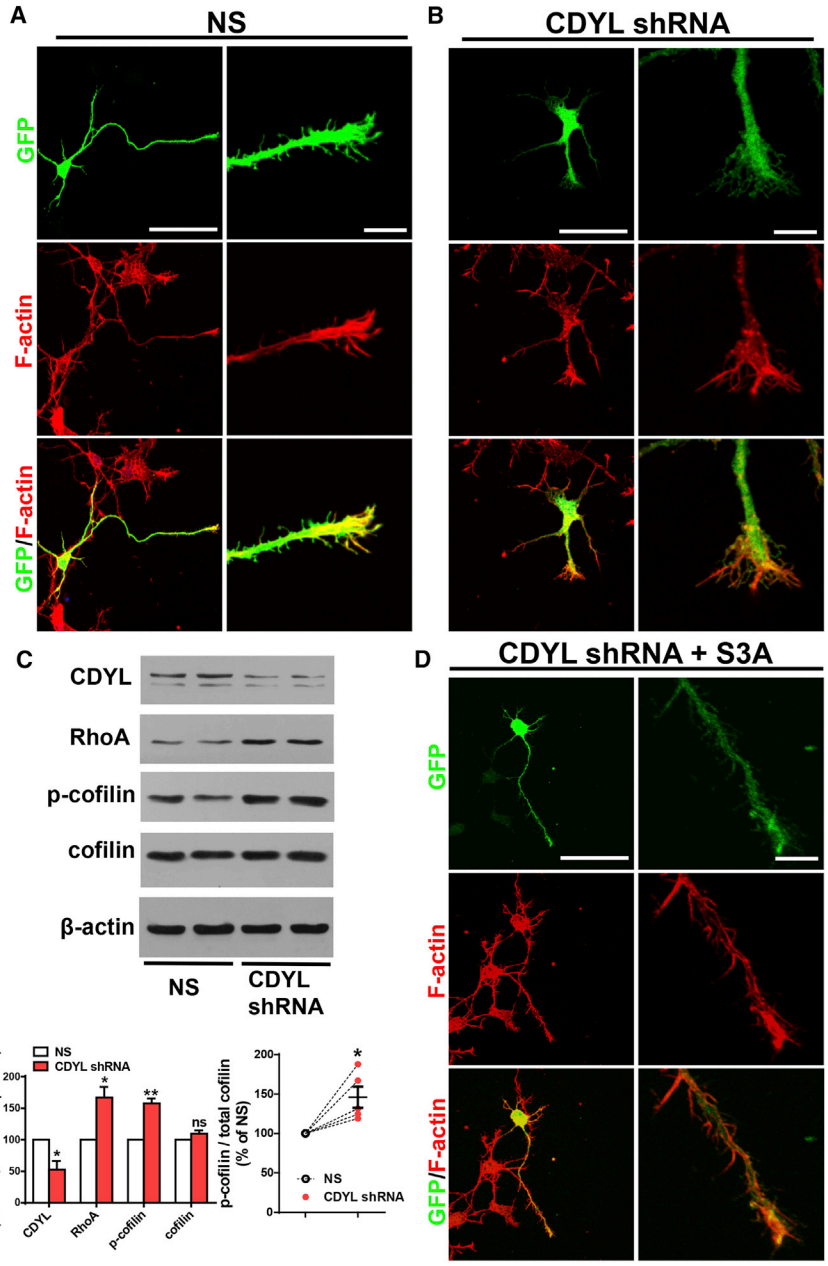

Figure 3. CDYL Promotes Neuronal Migration by Depolymerizing F-actin

(A and B) E14.5 mouse brains were in utero electroporated with NS (A) or CDYL shRNA (B) together with GFP. After 2 days, the brains were digested, and the cortical neurons were cultured. F-actin (red) was immunostained at 24 hr.

(C) Cortical neurons were transfected with NS or CDYL shRNA for 3 days. The protein levels of CDYL, RhoA, phosphorylated cofilin (p-cofilin), and total cofilin (cofilin) were examined by western blot. Quantification was shown below (left: level of each protein; right: proportion of phosphorylated cofilin). *$p < 0.05$; **$p < 0.01$; ns, no statistical significance; paired t test. Data are presented as mean ± SEM. The experiment was repeated at least three times.

(D) Overexpression of cofilin S3A stabilized the F-actin depolymerized by CDYL deficiency.

(A, B, and D) Scale bars, 50 μm (left); 10 μm (right).

ability and motor function, the swimming speeds were similar among mice with different genotypes (Figure S7F), indicating that the learning and retrieval of spatial memory are not affected in CDYL-deficient mice. Overall, CDYL shows its specificity in regulating the susceptibility to epilepsy without affecting motor ability, anxiety and fear emotions, spatial learning, and memory.

Knocking Down CDYL-Induced Neuronal Hyperexcitability

To explore why deletion of CDYL in cortical neurons leads to higher susceptibility to epilepsy, we tested neuronal excitability using whole-cell patch-clamp recording on the brain slices (P15–P20). Acute knockdown of CDYL in utero was adopted to exclude the possible presynaptic effects in *Cdyl* cKO mice, thus focusing on the postsynaptic mechanism alone. In recorded pyramidal neurons (Wang et al., 2015) (Figure 6A), the resting membrane potential (RMP) was unaffected (Figure 6B). However, knocking down CDYL increased the spontaneous spike frequency (Figures 6C and 6D) and changed the morphological patterns of spontaneous action potentials (APs); thus, the loss of CDYL produced firing instability in these neurons (Figures 6E–6G). These observations together suggest that the higher susceptibility to epilepsy observed in CDYL-deficient mice may be because of exploding neuronal firing that might be related with the abnormal firing patterns.

In general, increased neuronal firing results from strengthening of excitatory synaptic inputs and/or the intrinsic excitability of the neurons. We then asked which of the two possible reasons leads to the increased firing when knocking down CDYL. To address this question, we first recorded the spontaneous excitatory post-synaptic currents (sEPSCs). Interestingly, cortical excitatory neurons treated with CDYL shRNA showed decreased sEPSC frequencies and amplitudes compared with those of neurons with control shRNA (Figures 7A–7C), indicating that the synaptic inputs were weakened by knocking down postsynaptic CDYL. Next, we evoked APs by superimposed current steps to assess the passive membrane properties (Figure 7D), and found that the CDYL-knockdown neurons produced more APs and required relatively lower current intensity to induce APs (Figures 7E–7G), indicating that the intrinsic excitability was elevated in

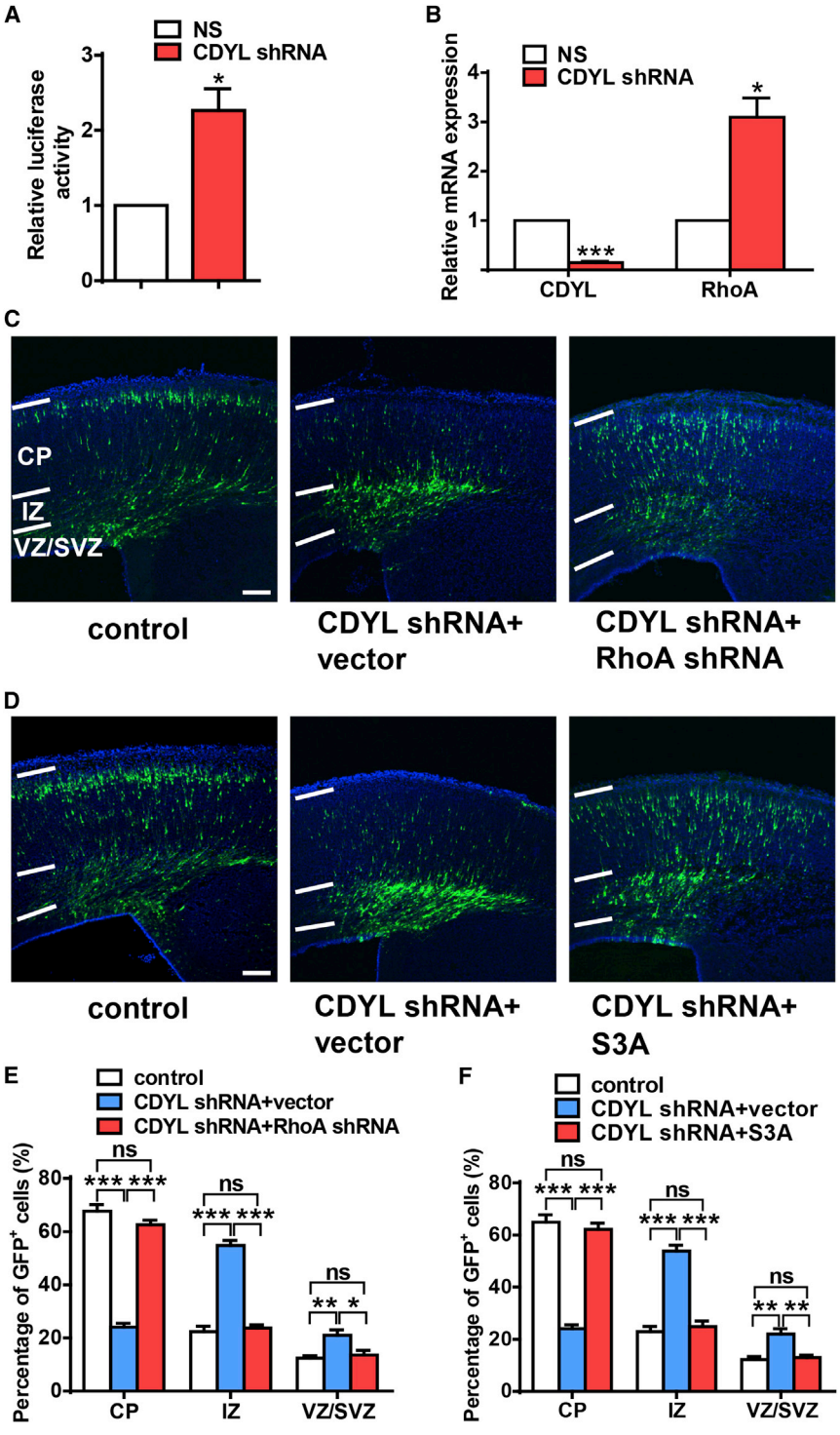

Figure 4. CDYL Regulates Neuronal Migration through RhoA-Cofilin Signaling

(A) N2a cells were transfected with the indicated plasmids for 48 hr and harvested for a RhoA luciferase reporter assay. *$p < 0.05$, paired t test.

(B) CDYL shRNA was transfected into cultured cortical neurons. Total RNA was extracted 48 hr later, and mRNA levels of RhoA and CDYL were measured by qPCR. *$p < 0.05$, ***$p < 0.001$, paired t test. The experiments of (A) and (B) were repeated at least three times.

(C) Representative E18.5 brain slices that were in utero electroporated with NS or CDYL shRNA along with vector or RhoA shRNA, respectively. The brains were cotransfected with GFP to visualize the distribution of the transfected neurons (green). Scale bar, 100 μm.

(D) Representative E18.5 brain slices that were in utero electroporated with NS or CDYL shRNA with vector or S3A cofilin, respectively. The brains were cotransfected with GFP to visualize the distribution of the transfected neurons (green), and cell nuclei were stained with Hoechst (blue). Scale bar, 100 μm.

(E and F) Quantification of the distribution of the GFP-positive neurons in (C) and (D), respectively. *$p < 0.05$; **$p < 0.01$; ***$p < 0.001$; ns, no statistical significance; two-way ANOVA with Tukey post hoc test. More than 1,000 GFP-positive neurons from three to five brains were analyzed in each group. Data are presented as mean ± SEM.

DISCUSSION

CDYL Is a Transcriptional Regulator of Neuronal Migration

Neuronal migration is one of the key determinants of brain development. Investigating the molecular and cellular mechanisms of neuronal migration is critical to understanding the formation of the six-layered structure of the cortex. CDYL, as a transcriptional repressor, has been reported to be involved in neural differentiation (Wan et al., 2013), and our previous study suggested that CDYL is a negative regulator of dendrite morphogenesis (Qi et al., 2014). In this study, we identified CDYL as a regulator of cortical neuronal migration. In utero electroporation of CDYL shRNA led to defects in cortical neuronal migration that could be rescued by the overexpression of shRNA-resistant CDYL, but not by the CDYL mutant lacking the chromodomain, indicating that the essential role of CDYL in neuronal migration depends on epigenetic regulation. In addition, CDYL is involved in the multipolar-to-bipolar transition shape in vivo. Consistent with the in vivo observation, we revealed that CDYL has an impact on early axonal elongation, as CDYL-knockdown neurons. These results demonstrate that knocking down CDYL leads to abnormal firing-dependent hypersusceptibility to seizures through upregulating the neuronal excitability rather than by strengthening excitatory synaptic inputs.

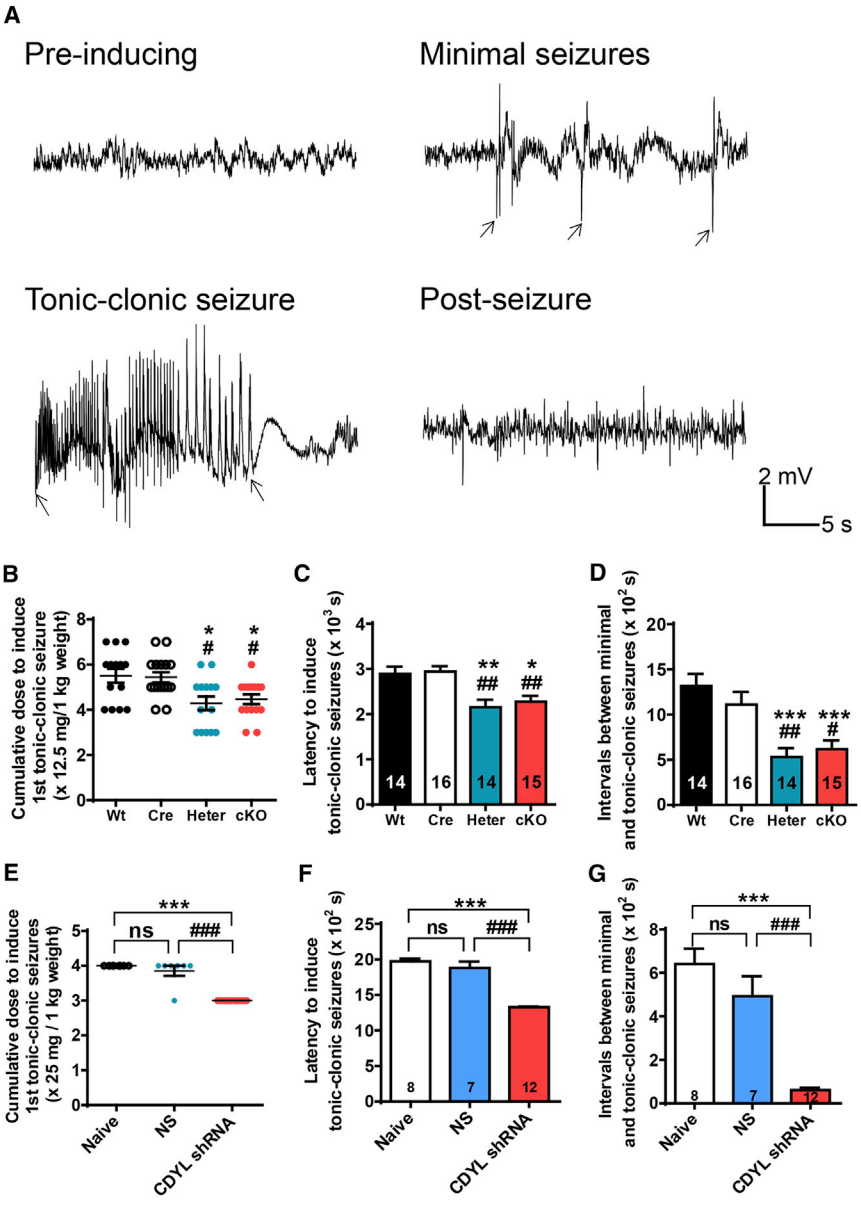

Figure 5. Loss of CDYL Increased the Susceptibility to PTZ-Induced Seizures

(A) Example traces matching the minimal and tonic-clonic seizures of PTZ-injected mice. Scale bars, 2 mV and 5 s. Arrows show the EEG patterns matching the behavioral events (upper right: events of minimal seizures; lower left: the onset and termination of a tonic-clonic seizure).

(B–D) PTZ was injected into C57BL/6 mice with the indicated genotypes once every 10 min. The latencies (B) and cumulative doses (C) required to induce the tonic-clonic seizures were lower in Heter and cKO mice. The intervals between minimal and tonic-clonic seizures (D) were also lower in Heter and cKO mice. WT, n = 14; Cre, n = 16; Heter, n = 14; cKO, n = 15; one-way ANOVA with post hoc Tukey test, $^{*}p < 0.05$, $^{**}p < 0.01$, $^{***}p < 0.001$ versus WT; $^{\#}p < 0.05$, $^{\#\#}p < 0.01$ versus Cre.

(E–G) PTZ was injected once every 10 min to ICR mice transfected in utero with control or CDYL shRNA at E14.5. The latencies (E) and cumulative doses (F) required to induce the tonic-clonic seizures and the intervals between minimal and tonic-clonic seizures (G) were lower in mice transfected with CDYL shRNA. Naive, n = 8; NS shRNA, n = 7; CDYL shRNA, n = 12; one-way ANOVA with post hoc Tukey test, $^{***}p < 0.001$ versus naive; $^{\#\#\#}p < 0.001$ versus NS. Data are presented as mean ± SEM.

observed in neurons cultured in vitro after in utero electroporation.

Both of these processes are regulated by cytoskeletal dynamics. Previous studies have thoroughly demonstrated that the regulation of RhoA activity contributes to regulating neuronal migration, but the regulation of the RhoA protein levels during neuronal migration is less clear. We find that the transcriptional corepressor, CDYL, regulates RhoA. Using a luciferase reporter assay, we found that the knockdown of CDYL increased RhoA transcription. In cultured neurons, CDYL knockdown increases both the mRNA and the protein levels of RhoA. In addition, CDYL knockdown increases the cofilin phosphorylation, and the migration defects observed after CDYL knockdown were rescued upon co-electroporation of RhoA shRNA or a constitutively active form of cofilin. Thus, we suggest that CDYL regulates neuronal migration through RhoA repression, subsequently inducing actin polymerization and eventually promoting neuronal migration.

CDYL acts as a reader protein by recognizing H3K27me3 and H3K9me2/3 (Mulligan et al., 2008; Zhang et al., 2011). Biochemical studies have demonstrated that CDYL can associate within the CtBP complexes (Shi et al., 2003), and CDYL connects the transcription repressor REST with the histone methyltransferase G9a (Mulligan et al., 2008). Furthermore, CDYL can recruit the histone deacetylases HDAC1 and HDAC2 to inhibit the transcription of its target genes (Caron et al., 2003). Previous work in our laboratory showed that CDYL recruited the H3K27 methyltransferase activity to repress BDNF transcription (Qi et al., 2014). All these studies suggest that CDYL is a corepressor of target gene transcription. Therefore, the partners and/or the epigenetic enzymes of CDYL in repressing RhoA and other target genes of CDYL during neuronal migration need to be studied in the future. Intriguingly, we noticed that the defects in neuronal migration in CDYL-deficient mice were not as significant as those induced upon in utero electroporation of CDYL shRNA. Similar phenomena have also been reported in other studies, including the neuronal migration regulators DCX and α2-chimaerin (Bai et al., 2003; Ip et al., 2011). Other factors may compensate for deficiency, and this possibility merits further investigation.

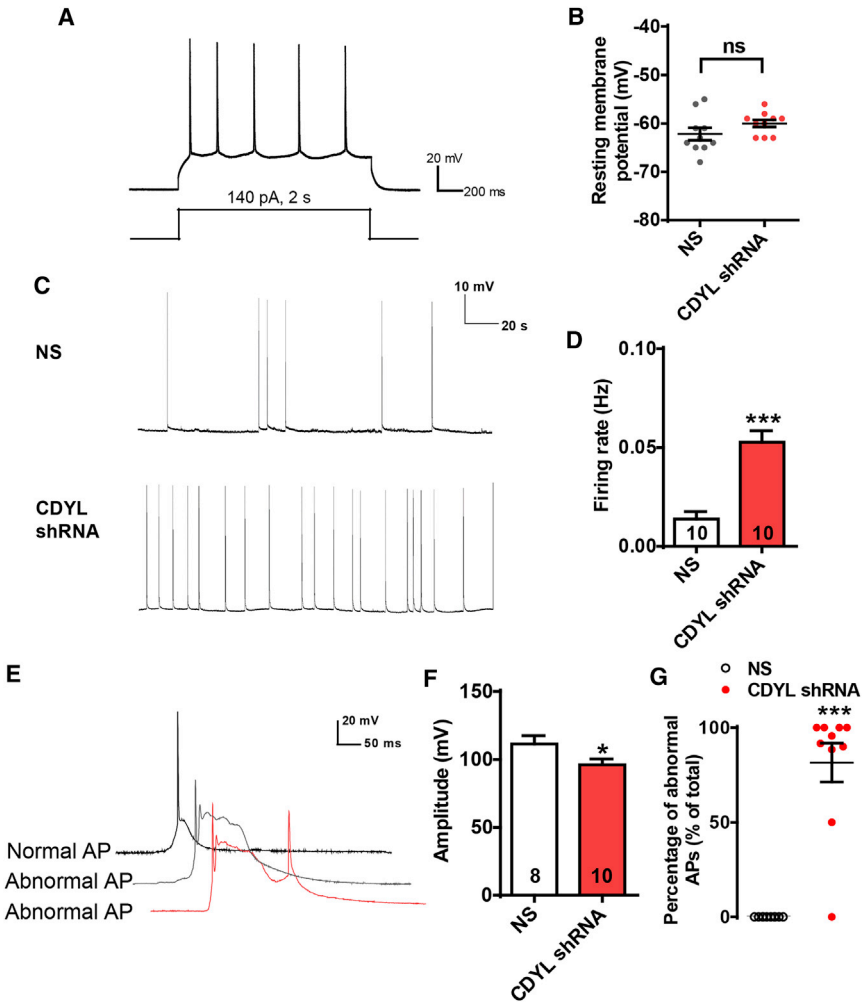

Figure 6. Knocking Down CDYL Leads to Abnormal Spontaneous Firing

(A) Current-clamp recordings to identify pyramidal excitatory neurons in the neocortex.

(B) The resting membrane potential was not affected by CDYL knockdown. Unpaired t test, n = 10, 10 neurons from at least five mice in each group.

(C) Representative recording traces of neurons from the mice in utero transfected with NS or CDYL shRNA. Scale bars, 10 V and 20 s, holding at −64 and −63 mV, respectively.

(D) Quantification of the spontaneous firing rates of neurons shown in (C). ***$p < 0.001$, unpaired t test, n = 10, 10 cells from at least five mice in each group.

(E) Representative patterns of action potentials (APs) of neurons from the mice in utero transfected with NS or CDYL shRNA. Abnormal APs showed a longer decay duration in which a follow-up AP occasionally occurred. Scale bars, 20 mV and 20 ms.

(F) The average amplitudes of APs in neurons transfected with NS or CDYL shRNA. *$p < 0.05$, unpaired t test, n = 8, 10 cells from at least five mice in each group.

(G) Proportions of abnormal APs among total spontaneous APs recorded in neurons transfected with NS or CDYL shRNA. Mann-Whitney test, ***$p < 0.001$, n = 10, 10 cells from at least five mice in each group. Data are presented as mean ± SEM.

The Dual Role of CDYL in Regulating Susceptibility to Epilepsy

As described above, the CDYL-deficient mice did not show significant motor disability and performed as well as the wild-type mice both in learning and memory tests and in other emotional tests. However, in the PTZ-induced seizure assay, CDYL-deficient mice showed a decreased latency of seizures. These results emphasize the specificity of CDYL in the regulation of susceptibility to epilepsy. Susceptibility to epilepsy correlates with both the stability of the neural network and the intrinsic neuronal homeostasis (Staley, 2015). According to our results, the specific role of CDYL in maintaining epileptic resistance might be an outcome of both neuronal network dynamics and individual properties functioning in parallel. On one hand, migration defects or altered cortical morphology can disrupt both local and long-range neuronal connections, leading to abnormal network activity (Jacobs et al., 1999; Paz and Huguenard, 2015). Thus, disrupting migration through CDYL deletion might impair cortical microcircuitry and lead to dysfunction of normal neuronal network dynamics. We have also found that CDYL knockdown increases the cortical neuronal excitability, and that the mechanism lies in the intrinsic hyperexcitability rather than in alterations in synaptic transmission because of the loss of CDYL. Taken together, the dual role of CDYL in regulating epileptic susceptibility might be one explanation for its specificity in restricting epileptic susceptibility.

Although there is substantial empirical evidence supporting the etiology of epilepsy in neuronal homeostasis, the molecular mechanisms are not well understood (Staley, 2015). Current clinical screening of epilepsy genes focuses on ion channels. However, the genes related to the epigenetic regulation of epilepsy are not well studied (Noebels, 2015). In the present study, abnormal firing patterns possibly indicate coherent dysfunction of multiple ion channels, such as Nav, Kv, and Cav channels. Our previous screen using a genome-wide microarray reveals the upregulation or downregulation of various Nav and Kv channels (Qi et al., 2014). Consistent with the screening results, the firing patterns (Figure 6E) showing lower amplitudes and longer decay durations in unstable oscillation are similar to those produced by aberrant Nav and Kv channels (combination of downregulations of sodium and potassium channels) (Noebels, 2015), suggesting that ion channel dysfunction results from transcriptional dysregulation caused by the loss of CDYL. Notably, and contrary to expectations, we have recorded decreased frequency and amplitude of sEPSCs in the CDYL knockdown neurons as evidence of fewer or weakened synaptic inputs. The reason for synaptic dysfunction might be that loss of CDYL

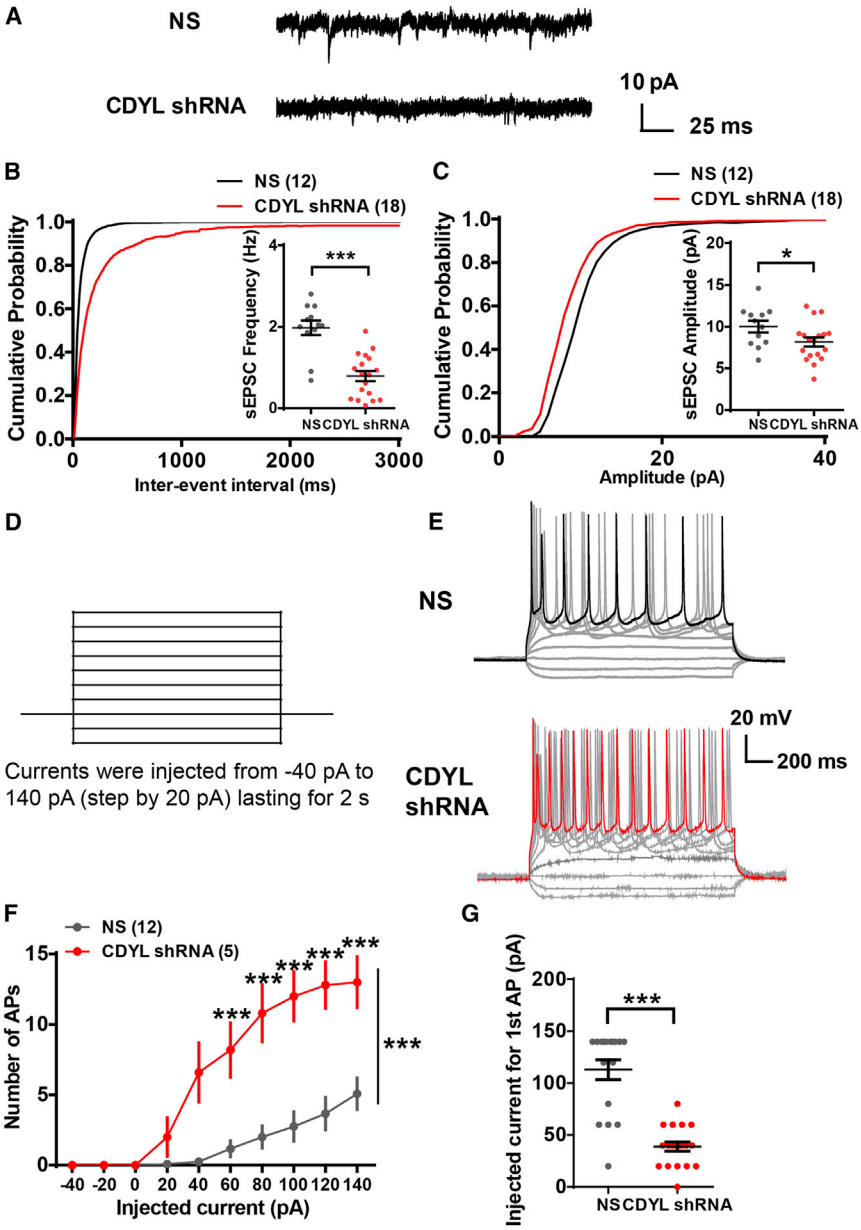

Figure 7. Knocking Down CDYL Leads to Neuronal Intrinsic Hyperexcitability

(A) Representative spontaneous excitatory postsynaptic currents (sEPSCs) of neurons transfected with NS or CDYL shRNA. Scale bars, 10 pA and 25 ms, holding at −60 mV.

(B and C) Cumulative probabilities (***$p < 0.001$ for B, *$p < 0.05$ for C, Kolmogorov-Smirnov two-sample test) and average sEPSC frequencies and amplitudes from the mice transfected with NS and CDYL shRNA. n = 12, 18 neurons from more than five mice for each group; *$p < 0.05$, ***$p < 0.001$, unpaired t test.

(D) Recording paradigm of passive excitability in the excitatory neocortical neurons.

(E) Examples of the AP responses to superimposed current steps recorded from pyramidal neurons from the mice transfected with NS or CDYL shRNA.

(F) Number of spikes induced by injected currents in the excitatory neurons from the mice transfected with NS or CDYL shRNA. n = 12, five neurons from five mice for each group; ***$p < 0.001$, two-way ANOVA with post hoc Tukey tests.

(G) Plot of the injected currents to induce the first spikes; 140 pA was set as the cutoff value. n = 17, 19 neurons from more than six mice for each group; ***$p < 0.001$, unpaired t test. Data are presented as mean ± SEM.

results in transcriptional dysregulation of synaptic proteins or in the failure of interneurons to form connections, because of disrupted migration. These findings partially support the idea that locally misplaced neurons, even only in small numbers, may result in an imbalance between excitatory and inhibitory synaptic activity and lead to epileptic seizures (Lapray et al., 2010).

Recently, CDYL has been reported to be upregulated in patients with Hirschsprung disease (HCSR), a neurodevelopmental disease (Enguix-Riego et al., 2016). However, whether the dysfunction of CDYL is relevant to epileptic seizures in human beings remains to be determined. Our findings have first identified CDYL as a single molecule involved in the dual regulation of epileptic susceptibility and have shed new light on the pathogenesis of neuropsychiatric disorders.

EXPERIMENTAL PROCEDURES

Mice

ICR and C57BL/6 mice were used throughout the experiments. All the mice were housed in a 12/12 hr light/dark cycle with their littermates (<6 in a vivarium). The *Cdyl* conditional knockout mouse model was created by Beijing Biocytogen. See Supplemental Experimental Procedures for generation of the *Cdyl* conditional knockout mouse model. All animal studies were approved by the Animal Center of the Peking University Health Science Center, and the methods were carried out in accordance with the relevant guidelines, including any relevant details.

Biochemistry

See the Supplemental Experimental Procedures for the procedures and materials (plasmids, antibodies, drugs, and others) for real-time PCR, western blotting, immunostaining, and RhoA reporter assay.

In Utero Electroporation

As previously described, E14.5 pregnant ICR mice were anesthetized by intraperitoneal injection with 0.7% sodium pentobarbital and checked for vaginal plugs. Mouse embryos were exposed in the uterus, and 1 μL DNA solution with 0.01% Fast Green was injected into the lateral ventricles of embryos. Plasmids were prepared in Milli-Q water at the concentrations of 1 μg/μL for GFP, 3 μg/μL for shRNAs, and 6 μg/μL for CDYL-R or CDYL del60-R. Electrical pulses of 36 V were generated with an Electro Squire portator T830 (BTX) and applied to the cerebral wall for 50 ms each, for a total of five pulses, at intervals of 950 ms. The uterus was then replaced, and the abdomen wall and skin were sutured. After surgical manipulation, mice were allowed to recover to consciousness in a 37°C incubator.

Cortical Slice Cultures and Live-Imaging Analysis

Mouse brains were in utero electroporated at E14.5 and then allowed to develop further for 3 days. Then electroporated brains were rapidly removed, and coronal slices (300 μm) were prepared using a Vibratome. Cortical slices were placed on Millicell-CM inserts (Millipore) in Neurobasal medium (Life Technologies) supplemented with 2% B27 (Life Technologies). Multiple GFP-positive cells were imaged on an inverted microscope (Olympus) with a 20× objective. Time-lapse images were captured at intervals of 6 min for 12 hr.

Primary Neuronal Cultures and Morphological Analysis

Cortical tissues isolated from embryonic day 16 mouse embryos were digested with 0.25% trypsin for 30 min at 37°C followed by triturating with a pipette in plating medium (DMEM with 10% FBS).

For electroporation, 3 × 10^6 cells were nucleofected with 6 μg plasmids (control or CDYL shRNA) as described by the manufacturer (Nepa Gene). Neurons were plated onto 35 mm dishes coated with poly-D-lysine (Sigma-Aldrich). After culturing for 4 hr, media were replaced with Neurobasal medium supplemented with 2% B27 and 0.5 mM GlutaMAX-I (Life Technologies). For studying morphology, cortical neurons were isolated 1 day after in utero electroporation at E14.5 with the control shRNA or CDYL shRNA together with GFP to label the transfected cells. After digestion, the cells were immediately plated on 35 mm dishes and then treated as above. Neurons were photographed at 20× magnification using an Olympus fluorescent microscope. The morphology of neurons in the cortex or culture was traced and analyzed using Neurolucida software (MBF Bioscience).

Behavioral Tests

At 8–10 weeks of age, male C57BL/6 mice of different genotypes were subjected to a set of behavioral tests to examine their emotional state and memory. In all of these experiments, mice were randomly coded to keep the experimenter and the analyzer blind. Each animal behavioral test was routinely performed at a specific time. Handling and habitation were performed as required before the experiments, and 70% ethanol was used to clear any possible odor cues after each test. See details in the Supplemental Experimental Procedures.

PTZ-Induced Seizures

As previously described (Ip et al., 2011), we used the convulsant agent pentylenetetrazol (PTZ; Sigma-Aldrich) to induce seizures in male ICR mice that had received in utero electroporation of non-silencing shRNA or CDYL shRNA at E14 (25 mg per kilogram body weight intraperitoneal administration every 10 min until generalized seizures occurred or until the cutoff latency of 3,600 s) and in male C57BL/6 mice whose genotypes were WT, Cre, Heter, or cKO (12.5 mg per kilogram body weight every 10 min considering the strain variation). The mice were examined for PTZ-induced seizures at P30–P45, when they weighed 20–30 g. The cumulative doses and latencies to induce the first minimal and tonic-clonic seizures (defined as head nodding with forelimb clonus and rearing paired with falling out of control, respectively) were recorded by video for each mouse. After the test, mice were sacrificed to confirm that each brain was intact and to confirm the successful delivery of shRNA by visualizing the distribution of GFP-positive cells. See details in the Supplemental Experimental Procedures for EEG recording procedures.

Whole-Cell Patch-Clamp Recordings

The methods for brain slice preparation and whole-cell patch-clamp recordings were similar to the protocols described previously (Wang et al., 2015). See details in the Supplemental Experimental Procedures.

Statistical Analysis

Data were analyzed and plotted using GraphPad Prism (version 6.00). Data that met the inclusion criteria would be examined to get eliminate outliers by ROUT method (Q was set as 0.05). Normality tests formally underwent the D'Agostino-Pearson omnibus normality test, and nonparametric tests were used for the data that failed the tests. All data underwent variance similarity tests. However, some data that failed the tests with variances within 3-fold (maximum/minimum) were still regarded as "similar variance." Statistical methods for comparisons were chosen properly from two-tailed t tests, one-way or two-way ANOVA followed by Bonferroni or Tukey post hoc tests. All data are presented as mean ± SEM.

SUPPLEMENTAL INFORMATION

Supplemental Information includes Supplemental Experimental Procedures, seven figures, and two movies and can be found with this article online at http://dx.doi.org/10.1016/j.celrep.2016.12.043.

AUTHOR CONTRIBUTIONS

Y.W. conceived and directed the project. R.Q. conducted the biochemical, morphological, and behavioral experiments, and analyzed the data. S.C. conducted electrophysiological and behavioral experiments, and analyzed the data. T.L., C.Q., and W.Z. partly conducted the experiments and analyzed the data. R.Q., S.C., T.L., C.Q., W.Z., and Y.W. discussed the data. R.Q., S.C., and Y.W. wrote the manuscript.

ACKNOWLEDGMENTS

We thank Dr. Huaye Zhang for RhoA shRNA constructs and Dr. Huikuan Lin for RhoA pGL-3 luciferase reporter constructs. We thank Dr. Dongmin Yin for discussions and critical reading of the manuscript. We thank Dr. Jiao Liu for the contribution to the Graphical Abstract. This work was supported by grants from the Ministry of Science and Technology of China (973 Program: grant 2014CB542204 to Y.W.) and the National Natural Science Foundation of China (grants 31530028, 91332119, 81161120497, 30925015, and 81521063 to Y.W.).

Received: September 12, 2016
Revised: November 6, 2016
Accepted: December 14, 2016
Published: January 10, 2017

REFERENCES

Ayala, R., Shu, T., and Tsai, L.H. (2007). Trekking across the brain: the journey of neuronal migration. Cell *128*, 29–43.

Azzarelli, R., Pacary, E., Garg, R., Garcez, P., van den Berg, D., Riou, P., Ridley, A.J., Friedel, R.H., Parsons, M., and Guillemot, F. (2014). An antagonistic interaction between PlexinB2 and Rnd3 controls RhoA activity and cortical neuron migration. Nat. Commun. *5*, 3405.

Bai, J., Ramos, R.L., Ackman, J.B., Thomas, A.M., Lee, R.V., and LoTurco, J.J. (2003). RNAi reveals doublecortin is required for radial migration in rat neocortex. Nat. Neurosci. *6*, 1277–1283.

Boitard, M., Bocchi, R., Egervari, K., Petrenko, V., Viale, B., Gremaud, S., Zgraggen, E., Salmon, P., and Kiss, J.Z. (2015). Wnt signaling regulates multipolar-to-bipolar transition of migrating neurons in the cerebral cortex. Cell Rep. *10*, 1349–1361.

Braat, S., and Kooy, R.F. (2015). The GABAA receptor as a therapeutic target for neurodevelopmental disorders. Neuron *86*, 1119–1130.

Cappello, S., Böhringer, C.R., Bergami, M., Conzelmann, K.K., Ghanem, A., Tomassy, G.S., Arlotta, P., Mainardi, M., Allegra, M., Caleo, M., et al. (2012). A radial glia-specific role of RhoA in double cortex formation. Neuron *73*, 911–924.

Caron, C., Pivot-Pajot, C., van Grunsven, L.A., Col, E., Lestrat, C., Rousseaux, S., and Khochbin, S. (2003). Cdyl: a new transcriptional co-repressor. EMBO Rep. *4*, 877–882.

Deutsch, S.I., Burket, J.A., and Katz, E. (2010). Does subtle disturbance of neuronal migration contribute to schizophrenia and other neurodevelopmental disorders? Potential genetic mechanisms with possible treatment implications. Eur. Neuropsychopharmacol. *20*, 281–287.

Enguix-Riego, M.V., Torroglosa, A., Fernández, R.M., Moya-Jiménez, M.J., de Agustín, J.C., Antiñolo, G., and Borrego, S. (2016). Identification of different

mechanisms leading to PAX6 down-regulation as potential events contributing to the onset of Hirschsprung disease. Sci. Rep. *6*, 21160.

Ge, W., He, F., Kim, K.J., Blanchi, B., Coskun, V., Nguyen, L., Wu, X., Zhao, J., Heng, J.I., Martinowich, K., et al. (2006). Coupling of cell migration with neurogenesis by proneural bHLH factors. Proc. Natl. Acad. Sci. USA *103*, 1319–1324.

Gleeson, J.G., and Walsh, C.A. (2000). Neuronal migration disorders: from genetic diseases to developmental mechanisms. Trends Neurosci. *23*, 352–359.

Govek, E.E., Newey, S.E., and Van Aelst, L. (2005). The role of the Rho GTPases in neuronal development. Genes Dev. *19*, 1–49.

Guerrini, R., and Parrini, E. (2010). Neuronal migration disorders. Neurobiol. Dis. *38*, 154–166.

Guo, H., Hong, S., Jin, X.L., Chen, R.S., Avasthi, P.P., Tu, Y.T., Ivanco, T.L., and Li, Y. (2000). Specificity and efficiency of Cre-mediated recombination in Emx1-Cre knock-in mice. Biochem. Biophys. Res. Commun. *273*, 661–665.

Ip, J.P., Shi, L., Chen, Y., Itoh, Y., Fu, W.Y., Betz, A., Yung, W.H., Gotoh, Y., Fu, A.K., and Ip, N.Y. (2011). α2-chimaerin controls neuronal migration and functioning of the cerebral cortex through CRMP-2. Nat. Neurosci. *15*, 39–47.

Jacobs, K.M., Kharazia, V.N., and Prince, D.A. (1999). Mechanisms underlying epileptogenesis in cortical malformations. Epilepsy Res. *36*, 165–188.

Jaglin, X.H., and Chelly, J. (2009). Tubulin-related cortical dysgeneses: microtubule dysfunction underlying neuronal migration defects. Trends Genet. *25*, 555–566.

Kriegstein, A.R., and Noctor, S.C. (2004). Patterns of neuronal migration in the embryonic cortex. Trends Neurosci. *27*, 392–399.

Lahn, B.T., and Page, D.C. (1999). Retroposition of autosomal mRNA yielded testis-specific gene family on human Y chromosome. Nat. Genet. *21*, 429–433.

Lahn, B.T., Tang, Z.L., Zhou, J., Barndt, R.J., Parvinen, M., Allis, C.D., and Page, D.C. (2002). Previously uncharacterized histone acetyltransferases implicated in mammalian spermatogenesis. Proc. Natl. Acad. Sci. USA *99*, 8707–8712.

Lapray, D., Popova, I.Y., Kindler, J., Jorquera, I., Becq, H., Manent, J.B., Luhmann, H.J., and Represa, A. (2010). Spontaneous epileptic manifestations in a DCX knockdown model of human double cortex. Cereb. Cortex *20*, 2694–2701.

Marín, O., and Rubenstein, J.L. (2003). Cell migration in the forebrain. Annu. Rev. Neurosci. *26*, 441–483.

Marín, O., Valdeolmillos, M., and Moya, F. (2006). Neurons in motion: same principles for different shapes? Trends Neurosci. *29*, 655–661.

Marín, O., Valiente, M., Ge, X., and Tsai, L.H. (2010). Guiding neuronal cell migrations. Cold Spring Harb. Perspect. Biol. *2*, a001834.

Morgan-Smith, M., Wu, Y., Zhu, X., Pringle, J., and Snider, W.D. (2014). GSK-3 signaling in developing cortical neurons is essential for radial migration and dendritic orientation. eLife *3*, e02663.

Mulligan, P., Westbrook, T.F., Ottinger, M., Pavlova, N., Chang, B., Macia, E., Shi, Y.J., Barretina, J., Liu, J., Howley, P.M., et al. (2008). CDYL bridges REST and histone methyltransferases for gene repression and suppression of cellular transformation. Mol. Cell *32*, 718–726.

Nadarajah, B., Brunstrom, J.E., Grutzendler, J., Wong, R.O., and Pearlman, A.L. (2001). Two modes of radial migration in early development of the cerebral cortex. Nat. Neurosci. *4*, 143–150.

Noebels, J. (2015). Pathway-driven discovery of epilepsy genes. Nat. Neurosci. *18*, 344–350.

Ota, H., Hikita, T., Sawada, M., Nishioka, T., Matsumoto, M., Komura, M., Ohno, A., Kamiya, Y., Miyamoto, T., Asai, N., et al. (2014). Speed control for neuronal migration in the postnatal brain by Gmip-mediated local inactivation of RhoA. Nat. Commun. *5*, 4532.

Pacary, E., Heng, J., Azzarelli, R., Riou, P., Castro, D., Lebel-Potter, M., Parras, C., Bell, D.M., Ridley, A.J., Parsons, M., and Guillemot, F. (2011). Proneural transcription factors regulate different steps of cortical neuron migration through Rnd-mediated inhibition of RhoA signaling. Neuron *69*, 1069–1084.

Paz, J.T., and Huguenard, J.R. (2015). Microcircuits and their interactions in epilepsy: is the focus out of focus? Nat. Neurosci. *18*, 351–359.

Qi, C., Liu, S., Qin, R., Zhang, Y., Wang, G., Shang, Y., Wang, Y., and Liang, J. (2014). Coordinated regulation of dendrite arborization by epigenetic factors CDYL and EZH2. J. Neurosci. *34*, 4494–4508.

Ridley, A.J., Schwartz, M.A., Burridge, K., Firtel, R.A., Ginsberg, M.H., Borisy, G., Parsons, J.T., and Horwitz, A.R. (2003). Cell migration: integrating signals from front to back. Science *302*, 1704–1709.

Shi, Y., Sawada, J., Sui, G., Affar, E.B., Whetstine, J.R., Lan, F., Ogawa, H., Luke, M.P., Nakatani, Y., and Shi, Y. (2003). Coordinated histone modifications mediated by a CtBP co-repressor complex. Nature *422*, 735–738.

Staley, K. (2015). Molecular mechanisms of epilepsy. Nat. Neurosci. *18*, 367–372.

Tabata, H., Kanatani, S., and Nakajima, K. (2009). Differences of migratory behavior between direct progeny of apical progenitors and basal progenitors in the developing cerebral cortex. Cereb. Cortex *19*, 2092–2105.

Tang, J., Ip, J.P., Ye, T., Ng, Y.P., Yung, W.H., Wu, Z., Fang, W., Fu, A.K., and Ip, N.Y. (2014). Cdk5-dependent Mst3 phosphorylation and activity regulate neuronal migration through RhoA inhibition. J. Neurosci. *34*, 7425–7436.

Tian, D., Diao, M., Jiang, Y., Sun, L., Zhang, Y., Chen, Z., Huang, S., and Ou, G. (2015). Anillin regulates neuronal migration and neurite growth by linking RhoG to the actin cytoskeleton. Curr. Biol. *25*, 1135–1145.

Tsai, L.H., and Gleeson, J.G. (2005). Nucleokinesis in neuronal migration. Neuron *46*, 383–388.

Wan, L., Hu, X.J., Yan, S.X., Chen, F., Cai, B., Zhang, X.M., Wang, T., Yu, X.B., Xiang, A.P., and Li, W.Q. (2013). Generation and neuronal differentiation of induced pluripotent stem cells in Cdyl-/- mice. Neuroreport *24*, 114–119.

Wang, G.Q., Cen, C., Li, C., Cao, S., Wang, N., Zhou, Z., Liu, X.M., Xu, Y., Tian, N.X., Zhang, Y., et al. (2015). Deactivation of excitatory neurons in the prelimbic cortex via Cdk5 promotes pain sensation and anxiety. Nat. Commun. *6*, 7660.

Zhang, Y., Yang, X., Gui, B., Xie, G., Zhang, D., Shang, Y., and Liang, J. (2011). Corepressor protein CDYL functions as a molecular bridge between polycomb repressor complex 2 and repressive chromatin mark trimethylated histone lysine 27. J. Biol. Chem. *286*, 42414–42425.

Cell Reports, Volume *18*

Supplemental Information

CDYL Deficiency Disrupts Neuronal Migration and Increases Susceptibility to Epilepsy

Rui Qin, Shuai Cao, Tianjie Lyu, Cai Qi, Weiguang Zhang, and Yun Wang

Supplemental Information

CDYL deficiency disrupts neuronal migration and increases susceptibility to epilepsy

Rui Qin, Shuai Cao, Tianjie Lyu, Cai Qi, Weiguang Zhang, Yun Wang

Supplemental Figures

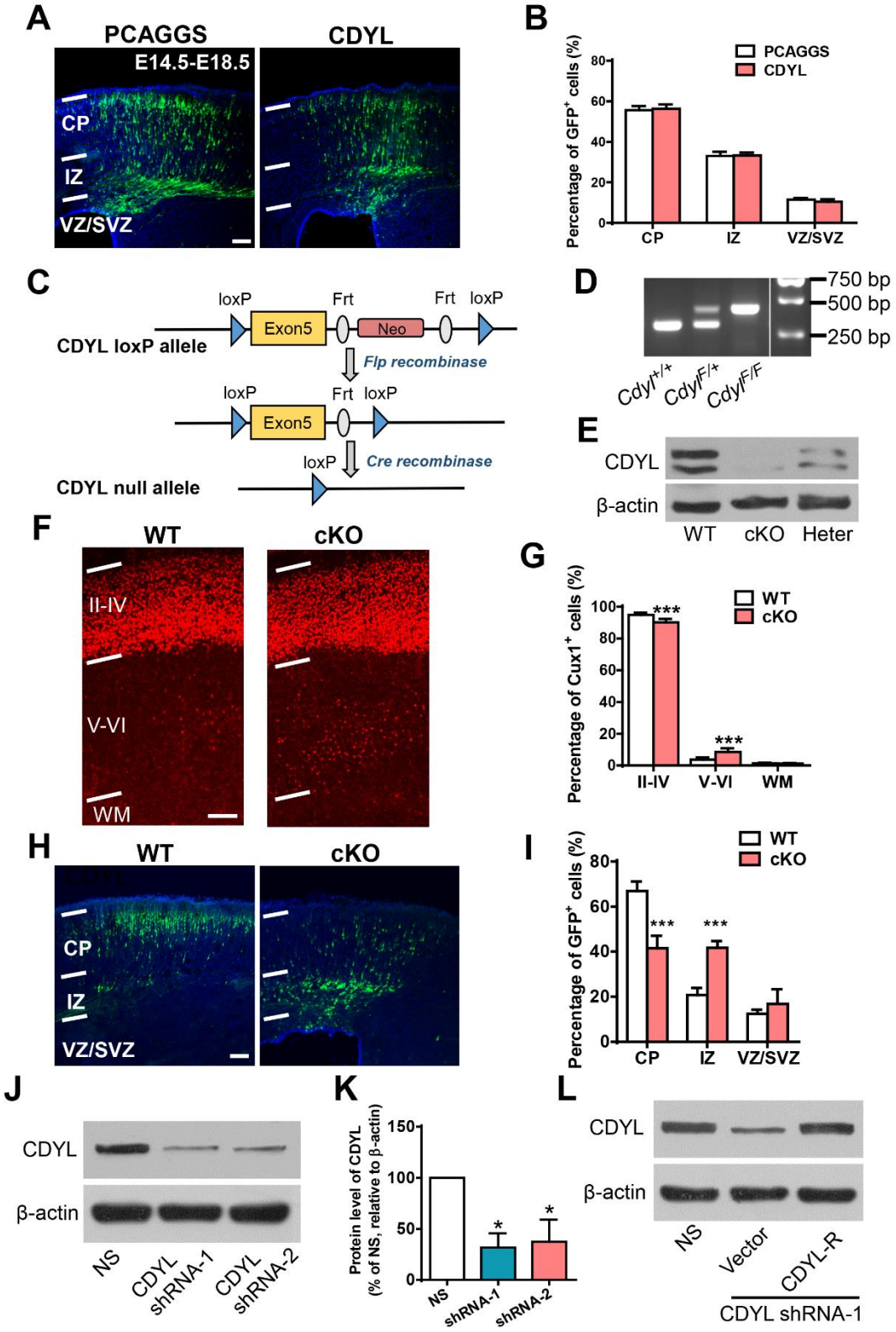

Figure S1 CDYL is important for neuronal migration, Related to Figure 1. (A)

Representative cerebral cortical sections from E18.5 mice were electroporated with

PCAGGS vectors (left) or CDYL (right) tagged with GFP (green) and quantification in **(B)**. Scale bar, 100 μm. No significant differences in CP, IZ, or VZ/SVZ between two groups, two-way ANOVA. **(C)** The strategy of conditional *Cdyl* knockout mice. **(D)** Genotyping of wild-type ($Cdyl^{+/+}$), heterozygous and homozygous genotypes ($Cdyl^{F/+}$, $Cdyl^{F/F}$) of the *Cdyl*-loxP mice by PCR. **(E)** CDYL expression in *Cdyl*-loxP, heterozygous and homozygous genotypes of the *Cdyl*-loxP mice crossed with *Emx1-Cre* mice (Wt, Heter and cKO, respectively). **(F)** The neocortex of Wt and CDYL cKO mice was stained for Cux1 (red) and quantification in **(G)**. Scale bar, 100 μm. In CDYL-deficient mice at P2, most Cux1-positive neurons are mislocalized to the deep cortical layers V/VI. ***$P < 0.001$, Wt versus cKO; two-way ANOVA with Tukey's post-hoc test. **(H)** Representative cerebral cortical sections from E18.5 Wt or cKO mice were electroporated with GFP (green) at E14.5 and quantification in **(I)**. Scale bar, 100 μm. ***$P < 0.001$, Wt versus cKO; two-way ANOVA with Tukey's post-hoc test. **(J)** Western blot showing the knockdown efficiency of CDYL shRNAs in N2a cells and quantification in **(K)**, *$P < 0.05$, repeated one-way ANOVA with Tukey's post-hoc test. **(L)** Western blot analysis showing that shRNA-resistant constructs of CDYL was generated. All the experiments were repeated for at least three times. The data are presented as the mean ± SEM.

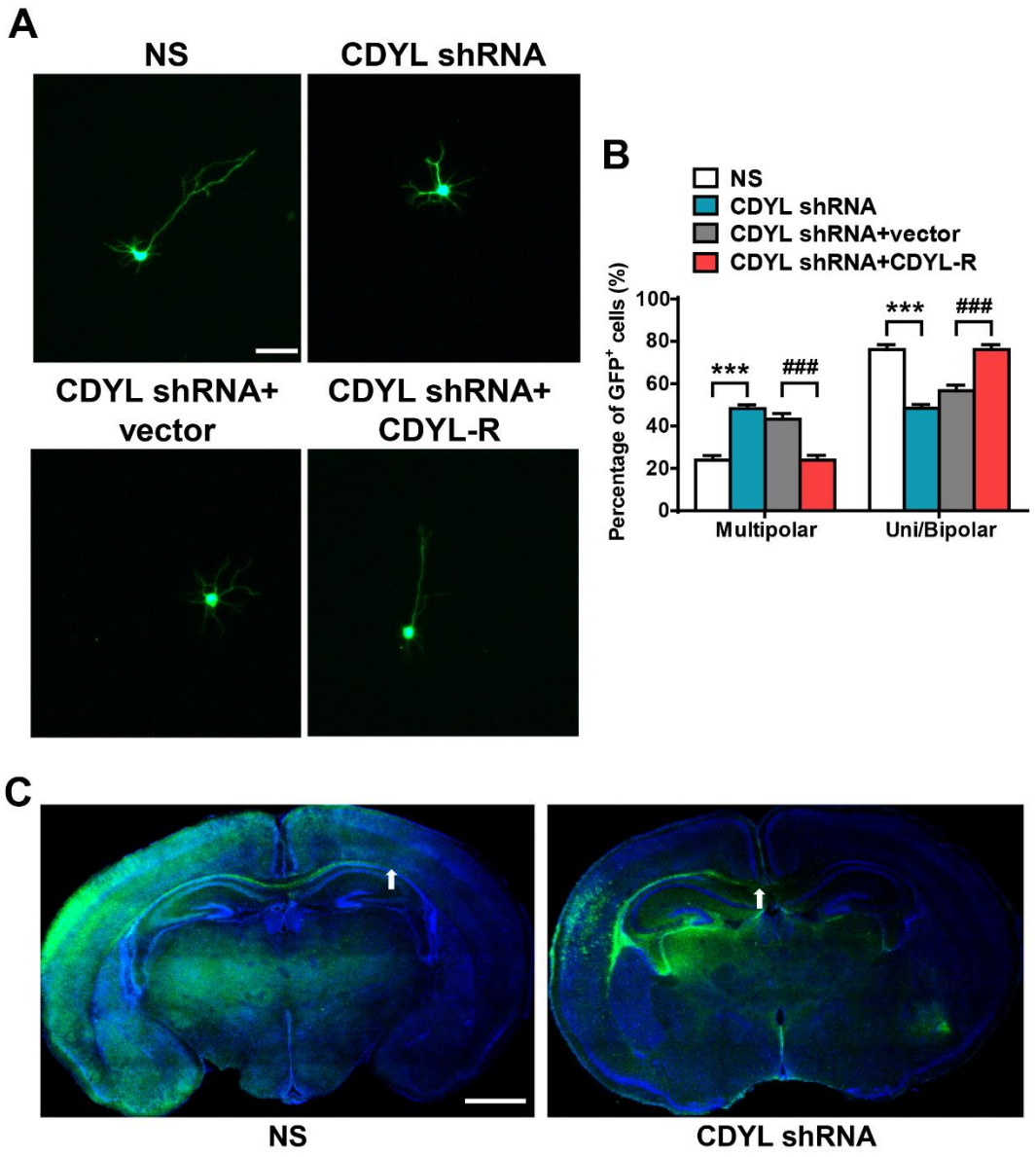

Figure S2 CDYL regulates the multipolar-bipolar transition *in vitro*, Related to Figure 2. (A) CDYL regulates neuronal morphology *in vitro*. E14.5 mouse brains were *in utero* electroporated with control, CDYL shRNA, CDYL shRNA + vector or CDYL shRNA + CDYL-R together with GFP. After 2 days, the brains were digested, and the cortical neurons were cultured for 3 days. Scale bar, 20 μm. **(B)** Quantification of the percentages of neurons with uni- or bipolar morphology and multipolar processes. The experiments were repeated three times, and more than 50

neurons were analyzed in each group. ***$P < 0.001$ compared to NS; ### $P < 0.001$ compared to CDYL shRNA + vector; two-way ANOVA with Tukey's post-hoc test. The data are presented as the mean ± SEM. **(C)** Representative images of slices from P7 mouse brain electroporated at E14.5 with plasmid expressing control or CDYL shRNA; and cell nuclei are stained with Hoechst (blue). Scale bar, 1 mm. Arrows show the locations of the longest axon terminals.

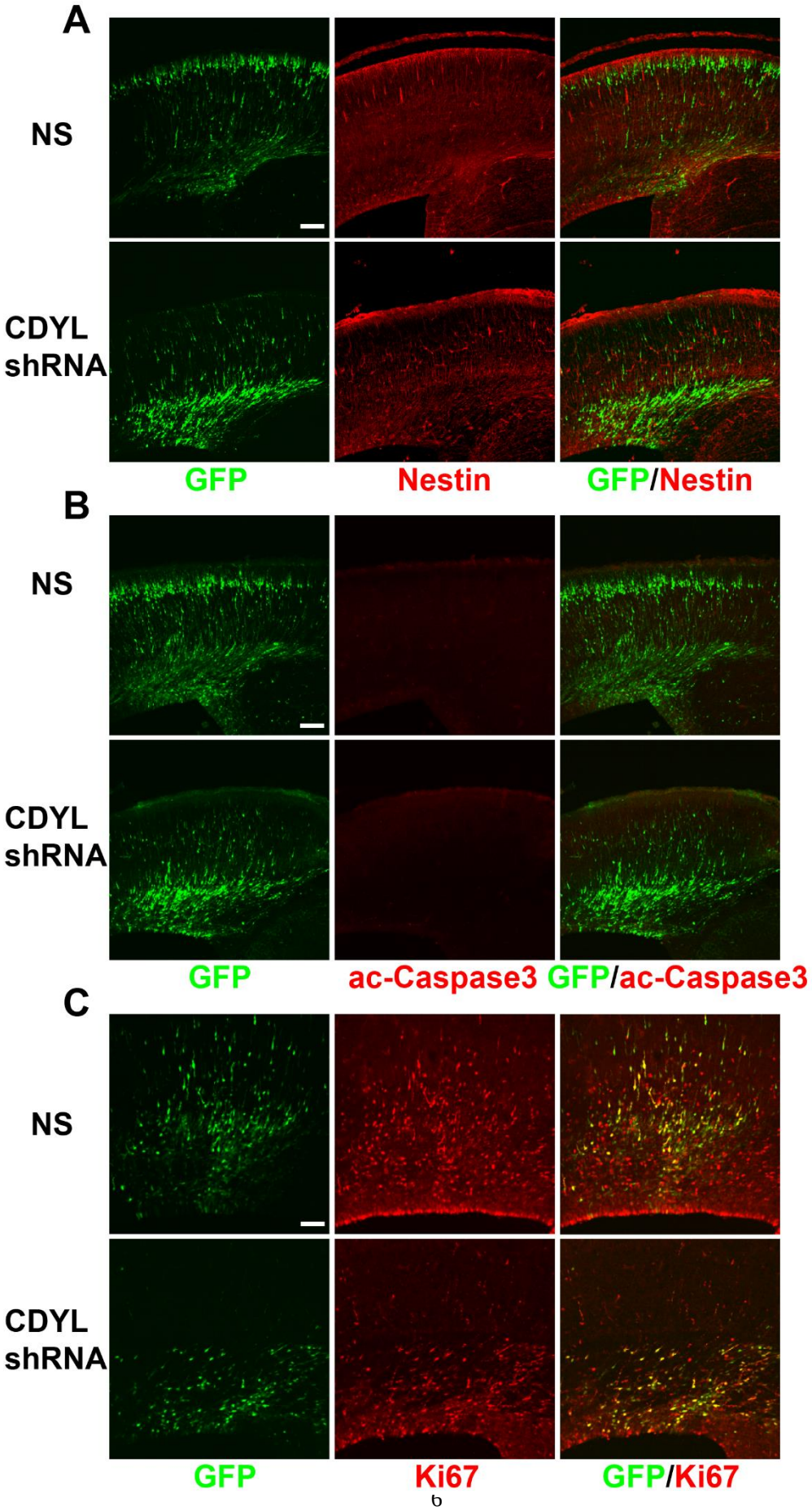
A
NS
CDYL shRNA
GFP
Nestin
GFP/Nestin
B
NS
CDYL shRNA
GFP
ac-Caspase3
GFP/ac-Caspase3
C
NS
CDYL shRNA
GFP
Ki67
GFP/Ki67

Figure S3 CDYL is dispensable for the radial glia scaffold, cell proliferation and apoptosis, Related to Figure 2. (A, B) Representative cerebral cortical sections from E18.5 mice were immunostained with antibodies against nestin (red in **A**) or cleaved Caspase-3 (ac-Caspase3, red in **B**) to label the radial glia scaffold or the cells undergoing apoptosis, respectively. Scale bar, 100 μm. **(C)** Representative images showing VZ/SVZ cells in E16.5 cortex immunostained for Ki67 (red). Embryonic brains were *in utero* electroporated with NS or CDYL shRNA at E14.5 together with GFP to label the transfected cells; scale bar, 50 μm.

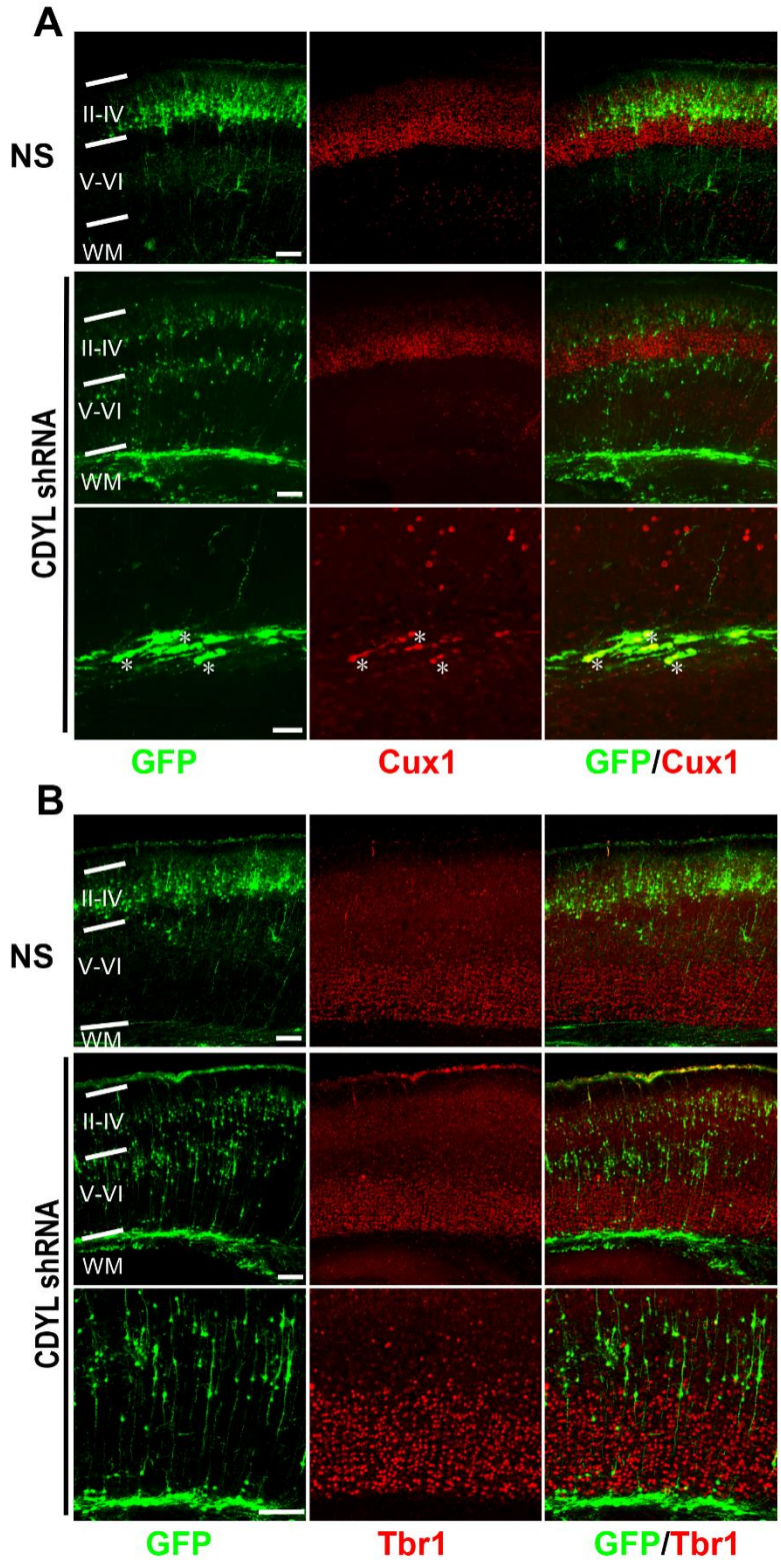

Figure S4 Loss of CDYL does not affect the density of cortical neurons, Related to Figure 2. (A and B) E14.5 mouse embryos were electroporated with NS or CDYL shRNA together with the GFP expression plasmid and allowed to develop until P7.

The cerebral cortex from the P7 mouse pups was subjected to immunofluorescent analyses for GFP and Cux1 (red in **A**. Scale bars, 100 μm in the top two panels, 20 μm in the lowest panel, asterisks indicate the colocalization of GFP-positive Cux1-positive neurons) or for GFP and Tbr1 (red in **B**. Scale bar, 100 μm) antibodies, cell nuclei were stained with Hoechst (blue).

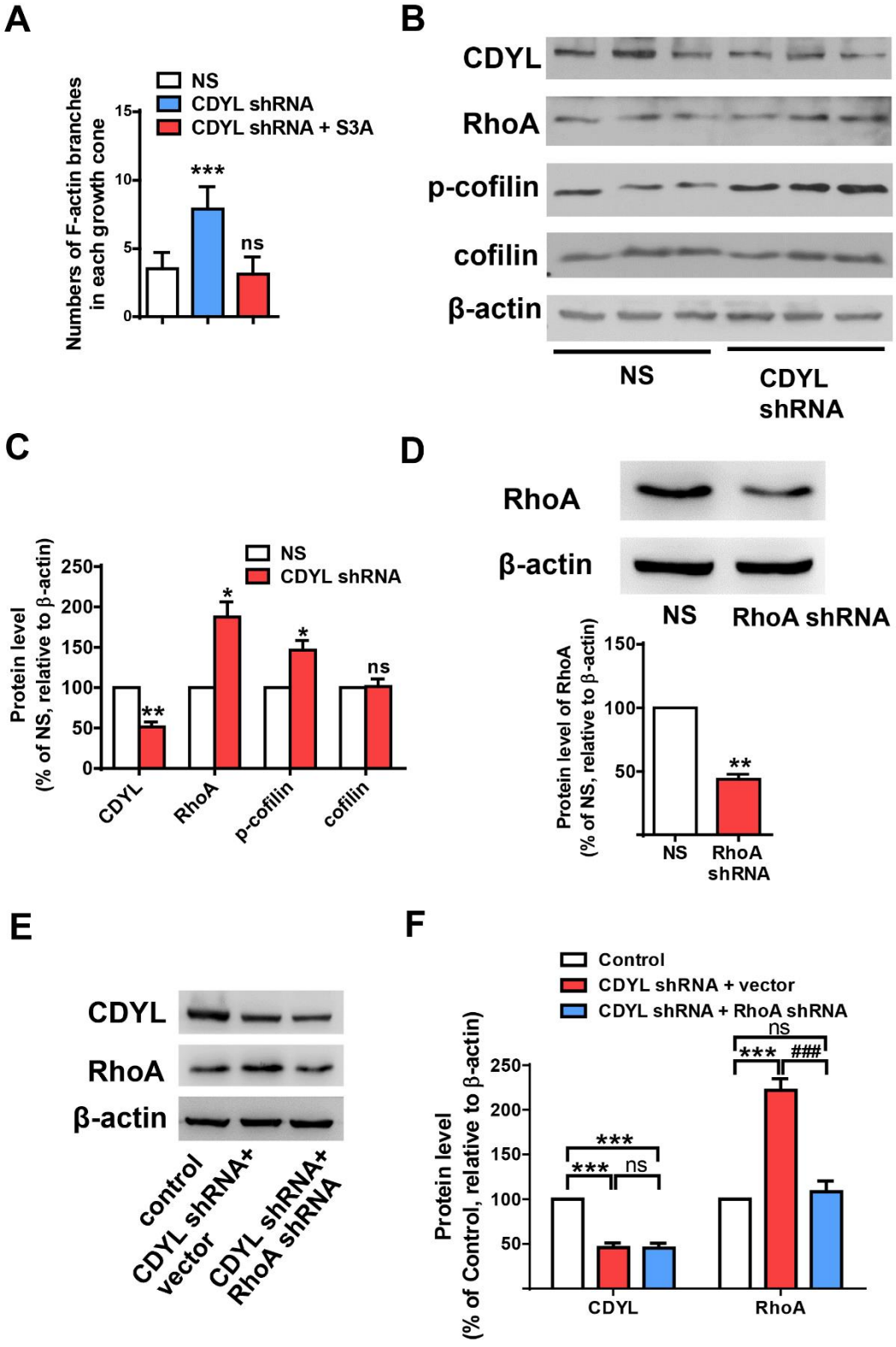

Figure S5 CDYL represses RhoA transcription, Related to Figure 3, 4. (A) Quantification of the F-actin branches in growth cones shown in Figure 3A, 3B, 3D. ***$P < 0.001$; ns, no statistical significance; one-way ANOVA with Tukey post hoc.

(B) NS or CDYL shRNA was transfected into N2a cells. The protein levels of CDYL, RhoA, phosphorylated cofilin and total cofilin were examined by Western blot 2 days later. **(C)** Quantification of **(B)**. *$P < 0.05$; **$P < 0.01$; ns, no statistical significance; paired t-test. **(D)** RhoA shRNA effectively knocked down RhoA expression. **$P < 0.01$, paired t-test. **(E)** CDYL shRNA with vector or RhoA shRNA were co-transfected into N2a cells. The protein levels of CDYL and RhoA were examined. **(F)** The quantification of each protein in **(E)**. *$P < 0.05$, **$P < 0.01$, ***$P < 0.001$, versus control; ###P < 0.001, versus CDYL shRNA + vector; ns, no statistical significance; repeated-measure one-way ANOVA with Tukey's post-hoc. These experiments were repeated for at least three times. The data are presented as the mean ± SEM.

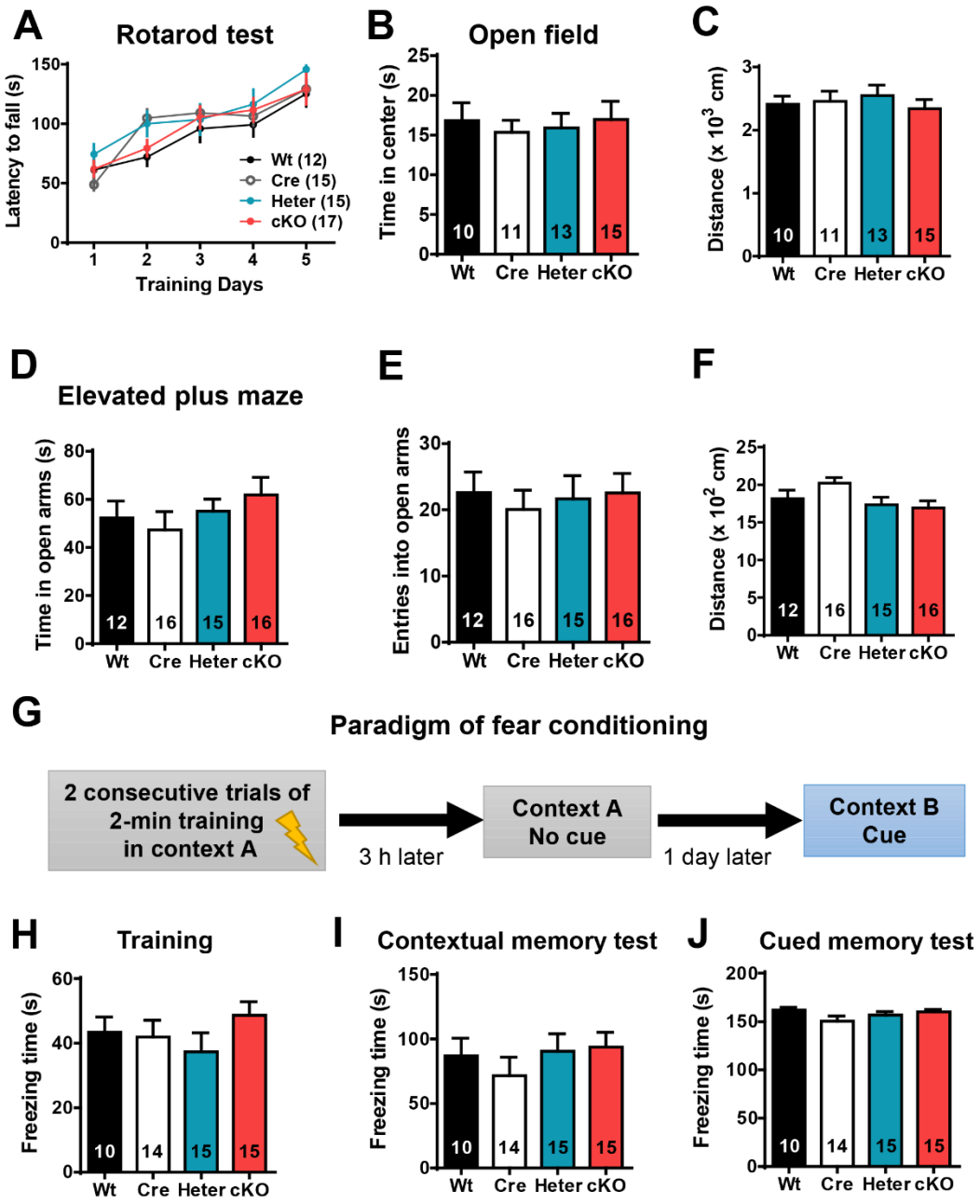

Figure S6 CDYL deficiency does not affect the motor function, the level of anxiety, or the fear conditioning of mice, Related to Figure 5. (A) Mice were tested for motor function and motor learning ability using the rotarod method. The latency for mice to fall off the rod was shown. n = 12, 15, 15 and 17 mice for the Wt, Cre, Heter and cKO groups, respectively. Two-way ANOVA, column factor P = 0.5091, interaction P = 0.0838. **(B-F)** Open field test and elevated plus maze test of mice with genotypes of Wt,

Cre, Heter and cKO to show their anxiety levels. One-way ANOVA, n = 10, 11, 13, 15 mice for the open field test **(B, C)** and 12, 16, 15, 16 for the elevated plus maze test **(D-F)**, $P > 0.05$. **(G-J)** Contextual and cue-dependent fear conditioning of mice with genotypes of Wt, Cre, Heter and cKO. The paradigm is shown in **(G)**. Total freezing times in the training period **(H)**, contextual test **(I)** and cue-dependent test **(J)** are shown. One-way ANOVA, n = 10, 11, 13, 15 mice, $P > 0.05$. The data are presented as the mean ± SEM.

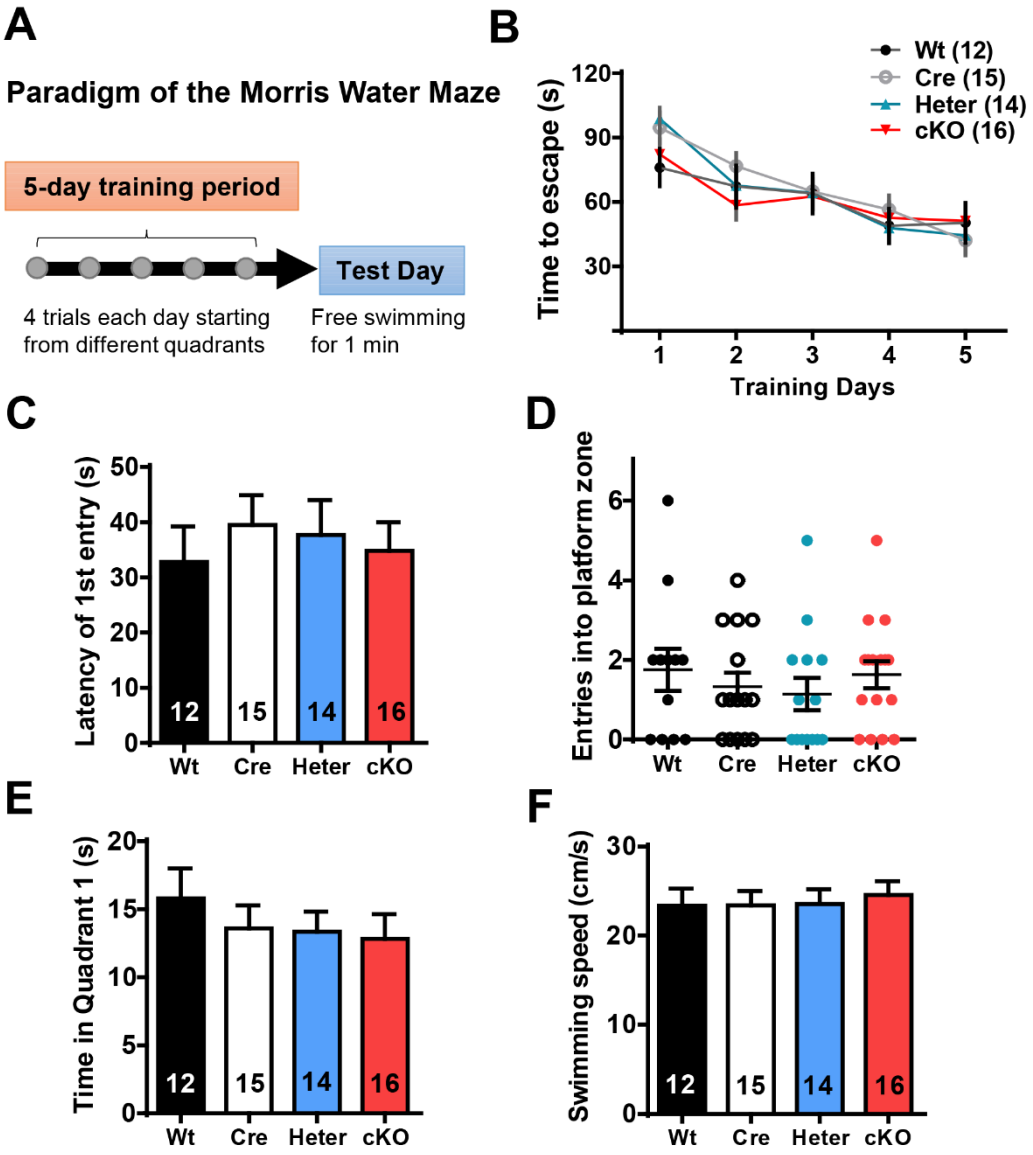

Figure S7 CDYL deficiency does not affect the spatial learning and memory of mice, Related to Figure 5. (A) The paradigm for the Morris water maze. **(B)** The escape times for the mice in the training trials. n = 12, 15, 14 and 16 mice for the Wt, Cre, Heter and cKO groups, respectively. Two-way ANOVA for the whole training phase, column factor $P = 0.8568$, interaction $P = 0.3238$. One-way ANOVA for the escape times of different genotypes on the 5th day of training, $P = 0.8134$. **(C-F)** The latencies to enter the platform zone **(C)**, total entries into the platform zone **(D)**, total time spent in the target quadrant **(E)** and the swimming speeds **(F)** of mice on the test

day. n = 12, 15, 14 and 16 mice for the Wt, Cre, Heter and cKO groups, respectively. One-way ANOVA, $P > 0.05$. The data are presented as the mean ± SEM.

Supplemental Movie Legends

Supplemental Movie S1, Related to Figure 2.

This movie shows an example of migrating neurons electroporated with NS shRNA and GFP plasmids. The neuron actively extended and retracted neurites, and it eventually formed one major leading process that guided the migration of cell body toward the pial surface. Images were captured every 6 min for 11 hours.

Supplemental Movie S2, Related to Figure 2.

This movie shows an example of migrating neurons electroporated with CDYL shRNA and GFP plasmids. The neuron showed impaired neurite dynamics and failed to form a leading process oriented toward the pial surface. Images were captured every 6 min for 11 hours.

Supplemental Experimental Procedures

Generation of the *Cdyl* conditional knockout mouse model.

The *Cdyl* conditional knockout mouse model was created by Beijing Biocytogen (Beijing, China). In brief, homologous regions covering 6.1 kb upstream of *Cdyl* exon 5 and 3.2 kb downstream of exon 5 were subcloned from a BAC clone (RP23-216H21; Invitrogen, Carlsbad, California, USA) from C57BL/6J mouse genomic BAC library. An FRT-flanked Neo-resistance positive-selection cassette was inserted downstream of exon 5, and two loxP sites were introduced in the upstream and downstream of exon 5, respectively. After linearization, the targeting vector was transfected into C57BL/6 embryonic stem (ES) cells (Biocytogen, Beijing, China) by electroporation. Seven positive clones were identified by Southern blotting with a 5' probe, a 3' probe and a 3' Neo probe. Three positive clones were injected into Balb/c blastocysts and implanted into pseudopregnant females. Chimeric mice were crossed with C57BL/6 mice to obtain F1 mice carrying the recombined allele containing the floxed *Cdyl* allele and the Neo selection cassette. To generate *Cdyl* conditional knockout mice, the mice carrying floxed alleles of *Cdyl* were crossed with *Emx1-Cre* mice (Guo et al., 2000) (Model Animal Research Center, Nanjing University, China). All animal studies were approved by the Animal Center of the Peking University Health Science Center, and the methods were carried out in accordance with the relevant guidelines, including any relevant details.

Plasmids

Doubled-stranded oligonucleotides were purchased and subcloned into the pSUPER vector. The shRNA sequences are as follows: CDYL shRNA-1 sense: 5'-GATCCCC-GGTACATCTCCATTCATGG-TTCAAGAGA-CCATGAATGGAGATGTACC-TTTTTA-3', antisense: 5'-AGCTTAAAAA-GGTACATCTCCATTCATGG-TCTCTTGAA-CCATGAATGGAGATGTACC-GGG-3'; CDYL shRNA-2 sense: 5'-GATCCCC-GAGATATTGTCGTCAGGAA-TTCAAGAGA-TTCCTGACGACAATATCTC-TTTTTA-3', antisense: 5'-AGCTTAAAAA-TTCCTGACGACAATATCTC-TCTCTTGAA-GAGATATTGTCGTCAGGAA-GGG-3'; non-silencing shRNA sense: 5'-GATCCCC-TTCTCCGAACGTGTCACGT-TTCAAGAGA-ACGTGACACGTTCGGAGAA-TTTTTA-3', antisense: 5'-AGCTTAAAAA-TTCTCCGAACGTGTCACGT-TCTCTTGAA-ACGTGACACGTTCGGAGAA-GGG-3'. Human CDYL and the indicated mutants (Qi et al., 2014), as well as S3A cofilin, were cloned into the pCAGGS-IRES-EGFP vector. The RhoA shRNA and RhoA pGL-3 luciferase reporter constructs were generous gifts from Dr. Huaye Zhang (Rutgers University, Piscataway, New Jersey, USA) and Dr. Huikuan Lin (The University of Texas MD Anderson Cancer Center, Houston, Texas, USA), respectively.

***In utero* electroporation**

As previously described, E14.5 pregnant ICR mice were anesthetized by intraperitoneal injection with 0.7% sodium pentobarbital and checked for vaginal plugs. Mouse

embryos were exposed in the uterus, and 1 μl of DNA solution with 0.01% Fast Green was injected into the lateral ventricles of embryos. Plasmids were prepared in Milli-Q water at the concentrations of 1 μg/μl for GFP, 3 μg/μl for shRNAs, and 6 μg/μl for CDYL-R or CDYL del60-R. Electrical pulses of 36 V were generated with an Electro Squire portator T830 (BTX, Holliston, Massachusetts, USA) and applied to the cerebral wall for 50 ms each, for a total of five pulses, at intervals of 950 ms. The uterus was then replaced, and the abdomen wall and skin were sutured. After surgical manipulation, mice were allowed to recover to consciousness in a 37 °C incubator.

Cortical slice cultures and live-imaging analysis

Mouse brains were *in utero* electroporated at E14.5 and then allowed to develop further for three days. Then, electroporated brains were rapidly removed, and coronal slices (300 μm) were prepared using a vibratome. Cortical slices were placed on Millicell-CM inserts (Millipore, Billerica, Massachusetts, USA) in Neurobasal medium (Life Technologies, Carlsbad, California, USA) supplemented with 2% B27 (Life Technologies, Carlsbad, California, USA). Multiple GFP-positive cells were imaged on an inverted microscope (Olympus, Tokyo, Japan) with a 20× objective. Time-lapse images were captured at intervals of 6 min for 12 h.

Primary neuronal cultures and morphological analysis

Cortical tissues isolated from embryonic day 16 mouse embryos were digested with 0.25% trypsin for 30 min at 37 °C followed by triturating with a pipette in plating

medium (DMEM with 10% FBS).

For electroporation, 3×10^6 cells were nucleofected with 6 μg of plasmids (control or CDYL shRNA) as described by the manufacturer (Nepa Gene, Ichikawa-City, Chiba, Japan). Neurons were plated onto 35 mm dishes coated with poly-D-lysine (Sigma-Aldrich, Munich, Germany). After culturing for 4 h, media were replaced with Neurobasal medium supplemented with 2% B27 and 0.5 mM GlutaMAX-I (Life Technologies, Carlsbad, California, USA). For studying morphology, cortical neurons were isolated one day after *in utero* electroporation at E14.5 with the control shRNA or CDYL shRNA together with GFP to label the transfected cells. After digestion, the cells were immediately plated on 35 mm dishes and then treated as above. Neurons were photographed at 20 × magnification using an Olympus fluorescent microscope. The morphology of neurons in the cortex or culture was traced and analyzed using Neurolucida software (MBF Bioscience, Williston, Vermont, USA).

Immunostaining

Mice were perfused with 4% paraformaldehyde (PFA) and fixed for 4-6 h (E14-P0 mice) or overnight (P7-adult mice) in 4% PFA at 4 °C. Fixed brains were cryoprotected in 20%–30% sucrose**,** embedded in Tissue-Tek O.C.T. compound (SAKURA, Torrance, California, USA), and then sectioned with a Leica 1950 cryostat.

For immunostaining, brain sections were washed three times with PBS and blocked for 1 hour at room temperature in 3% bovine albumin in 0.1 M PBS with 0.3% Triton X-100. Next, they were incubated with primary antibodies against Cux1 (1:200, Santa

Cruz, Dallas, Texas, USA), GFP (1:2,000, Roche, Basel, Switzerland), Tbr1 (1:1,000, Abcam, Cambridge, UK), Ki67 (1:1,000, Millipore, Billerica, Massachusetts, USA), Cleaved Caspase-3 (1:1,000, Cell Signaling Technology, Danvers, Massachusetts, USA), or Nestin (1:200, Millipore, Billerica, Massachusetts, USA) at 4 °C overnight and appropriate fluorescent secondary antibodies (Invitrogen, Carlsbad, California, USA) for 2 h at room temperature.

For F-actin labeling, cultured neurons were washed with 0.1 M PBS and then fixed in 4% PFA for 5 min. After washing, the neurons were permeabilized with 0.1% Triton X-100 in PBS and then incubated with a 50 μg/ml solution of rhodamine-labeled phalloidin (Sigma-Aldrich, Munich, Germany) in PBS for 40 min at room temperature. Finally, sections or neurons were counterstained with Hoechst 33342 (Sigma-Aldrich, Munich, Germany), and coverslips were applied. Images were acquired using either an FV-1200 (Olympus) or a TCS SP5 (Leica, Wetzlar, Germany) laser-scanning confocal microscope.

Real-time PCR

mRNA was isolated from independent samples using the RNeasy method (Invitrogen, Carlsbad, California, USA). After conversion into cDNAs using a Super Script First-Strand cDNA Synthesis kit (Invitrogen, Carlsbad, California, USA), quantitative RT-PCR was performed in a 96-well plate using an ABI 7500HT instrument. The relative expression of the related genes was analyzed by the ΔΔCt method (where Ct is the threshold cycle number) using *Gapdh* as a housekeeping gene. The following primers

were used: *Cdyl*: 5’-gacgctatcagaaacttcgtg-3’ (forward), 5’-acagcatttcattcgcaga-3’ (reverse); *RhoA*: 5’-cgtcggttctctccatagcc-3’ (forward), 5’-tcagatgcaaggctcaaggc-3’ (reverse); *Gapdh*: 5’-cttctgggtggcagtgat-3’ (forward), 5’-tggcaaagtggagattgtt-3’ (reverse).

Western blotting

Western blotting was performed according to protocols described previously (Wang et al., 2015a). In brief, tissues and cultured cells were homogenized in ice-cold lysis buffer (50 mM Tris, pH 7.4, 150 mM NaCl, 5 mM EGTA, 0.5% NP-40, 10 mM NaF, and 1 mM PMSF). The supernatant was extracted by centrifugation at 12,000 g at 4 °C for 5 min. Equal amounts of protein extracts were denatured and subjected to SDS–polyacrylamide gel electrophoresis. After separation, proteins were transferred to nitrocellulose membranes (Bio-Rad, Hercules, California, USA). Then, the membranes were probed with antibodies against CDYL (1:1,000, Proteintech, Rosemont, Illinois, USA), RhoA (1:200, Santa Cruz, Dallas, Texas, USA), p-cofilin (1:2,000, Santa Cruz, Dallas, Texas, USA), cofilin (1:1,000, Santa Cruz, Dallas, Texas, USA), and β-actin (1:10,000, Sigma-Aldrich, Munich, Germany).

RhoA reporter assay

HEK293 cells were transfected using Lipofectamine 2000 (Invitrogen, Carlsbad, California, USA) for 48 h, and luciferase activity was measured using the dual luciferase system (Promega, Madison, Wisconsin, USA). Each sample was analyzed in

triplicate, and experiments were performed at least three times. The relative luciferase activity was calculated as the ratio between firefly luciferase activity and Renilla luciferase activity.

Behavioral Tests

At 8–10 weeks of age, male C57BL/6 mice of different genotypes were subjected to a set of behavioral tests to examine their emotional state and memory. In all these experiments, mice were randomly coded to keep the experimenter and the analyzer blind. Handling and habitation were performed as required before the experiments, and 70% ethanol was used to clear any possible odor cues after each test.

Rotarod Test

Mice were tested for motor learning using the rotarod paradigm (Panlab, Barcelona, Spain). Examinations were performed 3 times per day, with intervals of 10−15 min, on 5 consecutive days. For each examination, the rod accelerated from 4 rpm to 40 rpm over 5 min, and it continued running at 40 rpm after 5 min. Mice were allowed to adapt for a few moments before each trial. The latency (in seconds) before the mouse fell off was recorded.

Elevated Plus Maze

The elevated plus maze was a cross-shaped platform at 50 cm above the floor with two open arms (30 cm × 5 cm) and two closed arms (30 cm × 5 cm × 40 cm) on opposing

sides of a central square platform (5 cm × 5 cm). The overall illuminations of the 4 arms were kept equal, at 100–200 lux. Each animal was gently placed in the center platform facing an open arm and was videotaped for 5 min. The total time and entries in the open arms (30 × 30 cm) and the distance the animals traveled were measured using the software SMART (version 2.5.21, Panlab, Barcelona, Spain).

Open Field Test

The apparatus was a white plastic open field with a square floor (60 cm × 60 cm) and surrounding walls (100 cm high). The overall illumination was kept at 100–200 lux. Each animal was gently placed in the center of the open field and videotaped for 5 min. The total time and entries in the center (30 × 30 cm) and the distance the animals traveled were measured using the software SMART (version 2.5.21, Panlab, Barcelona, Spain).

Morris Water Maze

The maze consisted of a round pool (diameter: 120 cm) and a round transparent plastic platform (diameter: 10 cm, placed at the center of the 1st quadrant, 1 cm below the water surface). The water was 50 cm deep and set at 23±2 °C. Patterns in different colors, shapes and combinations were used as visual cues for locating the hidden platform. Milk was added into the water to make it easier to trace the black mice. The Morris Water Maze test was performed as previously described (Vorhees and Williams, 2006). Briefly, we trained the mice for 4 trials per day with different start points for 5

consecutive days. The latency for each animal to find the platform (at least 3 sec stay) was recorded, and the cut-off value was set at 120 sec. On Day 6, the platform was removed, and animals searched freely for 1 min starting from the 3rd quadrant. The entries into the platform area, total time spent in the 1st quadrant, and the latencies to reach the platform were recorded using the software Morris (Mobile Datum, Shanghai, China). The animals with an average speed below 10 cm/sec were excluded for their weak motor ability.

Fear Conditioning Tests

A conditioning box (30 cm × 30 cm × 100 cm) with 2 different contexts (Mobile Datum, Shanghai, context A: black-and-white walls, metal net floor for electrical stimulation; context B: white walls and white plastic floor) was used for contextual and cued fear conditioning tests. Two rounds of training and two following conditioning tests were performed as described previously (Wu et al., 2012). Analysis was performed with the software Maze FCS (Mobile Datum, Shanghai, China). To measure the total freezing duration and frequency, 30 mm/s was set as the threshold of freezing.

EEG recording

Surgery was performed approximately 1 week prior to recordings, as previously described (Wang et al., 2014; Wang et al., 2015b). Briefly, under pentobarbital sodium anesthesia (0.5% w/v, 100 mg/kg), two stainless steel screws attached to insulated wire were implanted in the skull (approximately 0.5 mm anterior and 0.5 mm to the right/left

of bregma) over the frontal-parietal cortex for electroencephalography (EEG). Two ground electrodes were placed 0.8 mm lateral to the midline on each side. For the electrophysiological recordings, mice were placed in an electrically shielded box in a noise-attenuated environment with a light-weight shielded cable plugged into the connector on the mouse's head and attached to a counterbalanced swivel. The signals were routed to an electroencephalograph (model MP 150, BIOPAC Systems, Goleta, California, USA). Recordings and observation were performed for 30 min after the second injection (40 mg per kilogram body weight intraperitoneal administration, with an inter-injection interval of 10 min, 3.2-fold of the dose for measuring latencies of PTZ-induced seizures in order to shorten the recording). The signals were amplified, digitized at a sampling rate of 128 Hz, recorded using AcqKnowledge software (BIOPAC Systems, Goleta, California, USA), and plotted with GraphPad Prism (version 6.00, La Jolla, California, USA).

PTZ-induced Seizures

As previously described (Ip et al., 2012), we used the convulsant agent pentylenetetrazol (PTZ, Sigma-Aldrich, Munich, Germany) to induce seizures in male ICR mice that had received *in utero* electroporation of non-silencing shRNA or CDYL shRNA at E14 (25 mg per kilogram body weight intraperitoneal administration every 10 min until generalized seizures occurred or until the cut-off latency of 3600 sec), and in male C57BL/6 mice whose genotypes were Wt, Cre, Heter or cKO (12.5 mg per kilogram body weight every 10 min considering the strain variation). The mice were

examined for PTZ-induced seizures at P30−P45, when they weighed 20−30 g. The cumulative doses and latencies to induce the first minimal and tonic-clonic seizures were recorded by video for each mouse. Briefly, the head nodding with forelimb clonus and rearing paired with falling out of control were used as the marker behaviors for minimal seizures and tonic-clonic seizures, respectively. The protocol was repeatable in two strains of mice (both ICR and C57BL/6). To ensure the validity of this method, we underwent EEG experiments only to point out that PTZ-induced seizures showed coupling of the EEG pattern and marker behaviors (Figure. 5A). After the test, mice were sacrificed to confirm that the brain was intact and to confirm the successful delivery of shRNA by visualizing the distribution of GFP-positive cells.

Whole-cell patch clamp recordings

The methods for brain slice preparation and whole-cell patch clamp recordings were similar to the protocols described previously (Wang et al., 2015a). Mice (15–20 days old) were anesthetized with pentobarbital sodium (40 mg/kg, i.p.). The brains were quickly removed (within 1 min) and submerged in ice-cold dissection fluid that contained the following (in mM): 213 sucrose, 3 KCl, 0.5 $CaCl_2$, 5 $MgCl_2$, 1 NaH_2PO_4, 26 $NaHCO_3$, and 10 glucose (saturated with 95% O_2–5% CO_2). Coronal bilateral slices (300 μm in thickness) that contained the cerebral cortex were then cut on a Vibroslice (1000+, Pelco 102, Ted Pella, Redding, California, USA) and incubated in an oxygenated (95% O_2–5% CO_2) artificial cerebrospinal fluid (ACSF) that consisted of the following (in mM): 125 NaCl, 5 KCl, 2.6 $CaCl_2$, 1.3 $MgCl_2$, 1.2 NaH_2PO_4, 26

$NaHCO_3$, and 10 glucose (saturated with 95% O_2–5% CO_2). Each slice was kept at room temperature (approximately 23 °C) for at least 0.5 h before being transferred to the recording chamber. The chamber was perfused with ACSF at 2–3 mL/min using a pump (Peri-Star 291, World Precision Instruments, Sarasota, Florida, USA).

A slice was viewed with an upright microscope (Axioskop Fsmot, Zeiss, Germany) equipped with infrared-differential interference contrast (IR-DIC) optics. The recording pipettes (4–10 MΩ) were filled with solution that contained (in mM): 140 K-gluconate, 8 NaCl, 2 $MgCl_2$, 1 EGTA, 10 HEPES, 2 Mg-ATP, and 0.3 Na-GTP (adjusted to pH 7.2 with KOH, 290–320 mOsm). Voltage and current signals were recorded primarily from neurons with fluorescence. Note that the neurons we patched were either ectopic or seemingly normal-localized. The spike-firing pattern of the action potentials was used for electrophysiological identification of pyramidal neurons, which exhibited significant spike frequency adaptation in response to a depolarization current. The series resistance (Rs) was monitored at regular intervals throughout the recording experiment. Cells with Rs greater than 30 MΩ during the recordings were discarded. The neurons with a resting membrane potential below -55 mV were excluded. The action potentials (AP) were recorded using the current-clamp mode, spontaneous spikes in free-gap and induced APs were evoked by superimposed current steps. Data were acquired and analyzed with the Axoclamp 200B amplifier and pCLAMP software (Axon Instruments, Foster City, California, USA). For sEPSC recordings, picrotoxin (50 μM) was added to block $GABA_A$ receptor-mediated inhibitory synaptic currents. The sEPSCs were recorded for 5 min using the voltage-clamp mode, and neurons were

voltage clamped at -60 mV. The analysis of sEPSCs was performed blind using MiniAnalysis software (Synaptosoft, Decatur, Georgia, USA). The average amplitude and frequency of sEPSCs was determined using two-tailed t-tests. The cumulative distributions of sEPSCs were compared using a Kolmogorov–Smirnov two-sample test. $P < 0.05$ was considered to be statistically significant. Data are presented as the mean ± SEM.

Statistical analysis

Data were analyzed and plotted using GraphPad Prism (version 6.00, La Jolla, California, USA). Data which met the inclusion criteria would be examined to get rid of outliers by ROUT method (Q was set as 0.05). Normality tests were formally underwent using D'Agostino-Pearson omnibus normality test and nonparametric tests were used for the data which failed the tests. Variance similarity tests were formally underwent for all data. However, some data which failed the tests with variances within 3 folds (max/min) were still regarded as "similar variance". Statistical methods for comparisons were chosen properly from two-tailed t-tests, one-way or two-way ANOVA followed by Bonferroni or Tukey post-hoc tests. All data are presented as mean ± SEM.

Supplemental References

Guo, H., Hong, S., Jin, X.L., Chen, R.S., Avasthi, P.P., Tu, Y.T., Ivanco, T.L., and Li, Y. (2000). Specificity and efficiency of Cre-mediated recombination in Emx1-Cre knock-in mice. Biochem Biophys Res Commun *273*, 661-665.

Ip, J.P., Shi, L., Chen, Y., Itoh, Y., Fu, W.Y., Betz, A., Yung, W.H., Gotoh, Y., Fu, A.K., and Ip, N.Y. (2012). alpha2-chimaerin controls neuronal migration and functioning of the cerebral cortex through CRMP-2. Nat Neurosci *15*, 39-47.

Qi, C., Liu, S., Qin, R., Zhang, Y., Wang, G., Shang, Y., Wang, Y., and Liang, J. (2014). Coordinated regulation of dendrite arborization by epigenetic factors CDYL and EZH2. The Journal of neuroscience : the official journal of the Society for Neuroscience *34*, 4494-4508.

Vorhees, C.V., and Williams, M.T. (2006). Morris water maze: procedures for assessing spatial and related forms of learning and memory. Nat Protoc *1*, 848-858.

Wang, G.Q., Cen, C., Li, C., Cao, S., Wang, N., Zhou, Z., Liu, X.M., Xu, Y., Tian, N.X., Zhang, Y., *et al.* (2015a). Deactivation of excitatory neurons in the prelimbic cortex via Cdk5 promotes pain sensation and anxiety. Nat Commun *6*, 7660.

Wang, Z.J., Yu, B., Zhang, X.Q., Sheng, Z.F., Li, S.J., Huang, Y.L., Cao, Q., Cui, X.Y., Cui, S.Y., and Zhang, Y.H. (2014). Correlations between depression behaviors and sleep parameters after repeated corticosterone injections in rats. Acta Pharmacol Sin *35*, 879-888.

Wang, Z.J., Zhang, X.Q., Cui, X.Y., Cui, S.Y., Yu, B., Sheng, Z.F., Li, S.J., Cao, Q., Huang, Y.L., Xu, Y.P., *et al.* (2015b). Glucocorticoid receptors in the locus coeruleus mediate sleep disorders caused by repeated corticosterone treatment. Sci Rep *5*, 9442.

Wu, Q.F., Yang, L., Li, S., Wang, Q., Yuan, X.B., Gao, X., Bao, L., and Zhang, X. (2012). Fibroblast growth factor 13 is a microtubule-stabilizing protein regulating neuronal polarization and migration. Cell *149*, 1549-1564.